



UNIVERSIDAD NACIONAL AUTÓNOMA DE MÉXICO
POSGRADO EN CIENCIAS FÍSICAS

ON THE DETERMINATION OF TWO-BODY MATRIX
ELEMENTS FROM LATTICE FIELD THEORIES

TESIS

QUE PARA OPTAR POR EL GRADO DE:

MAESTRO EN CIENCIAS (FÍSICA)

P R E S E N T A

MARCO ANTONIO CARRILLO BERNAL

TUTORES PRINCIPALES

DR. RAÚL BRICEÑO

OLD DOMINION UNIVERSITY Y JEFFERSON LAB

DR. WOLFGANG PETER BIETENHOLZ

INSTITUTO DE CIENCIAS NUCLEARES

MIEMBROS DEL COMITÉ TUTOR

DR. GENARO TOLEDO SÁNCHEZ

INSTITUTO DE FÍSICA

DR. PAUL ARTUR JENS ERLER WEBER

INSTITUTO DE FÍSICA

CIUDAD DE MÉXICO, NOVIEMBRE 2019



Universidad Nacional
Autónoma de México



UNAM – Dirección General de Bibliotecas
Tesis Digitales
Restricciones de uso

DERECHOS RESERVADOS ©
PROHIBIDA SU REPRODUCCIÓN TOTAL O PARCIAL

Todo el material contenido en esta tesis esta protegido por la Ley Federal del Derecho de Autor (LFDA) de los Estados Unidos Mexicanos (México).

El uso de imágenes, fragmentos de videos, y demás material que sea objeto de protección de los derechos de autor, será exclusivamente para fines educativos e informativos y deberá citar la fuente donde la obtuvo mencionando el autor o autores. Cualquier uso distinto como el lucro, reproducción, edición o modificación, será perseguido y sancionado por el respectivo titular de los Derechos de Autor.

Resumen

Lattice QCD (LQCD) ofrece un marco de trabajo no perturbativo que permite el estudio de sistemas hadrónicos mediante el uso de herramientas computacionales. La mayoría de estados hadrónicos decaen fuertemente a estados de multipartículas, es decir, son estados resonantes. Con el propósito de extender las aplicaciones de las teorías cuánticas de campo en la red, el formalismo Briceño-Hansen establece una relación entre los elementos de matriz de corrientes externas, los cuales se obtienen a través de la red, con las correspondientes amplitudes de transición de estados de dos partículas en un volumen infinito. En el campo de física nuclear, este formalismo daría pie al análisis de estructuras de estados hadrónicos de dos partículas por medio de LQCD. Esto incluye estados resonantes, como glueballs y pentaquarks, y estados ligados, como el deuterón. Debido a que los estudios en LQCD requieren una gran cantidad de tiempo y recursos computacionales, en esta tesis exploramos la aplicación del formalismo Briceño-Hansen para un modelo de dos modelos de Ising acoplados. Observamos que es posible definir una corriente de transición en términos de los operadores del modelo para extraer los elementos de matriz de estados de una partícula. El paso siguiente será extraer los elementos de matriz de estados de dos partículas, lo cual proporcionaría las piezas necesarias para probar el formalismo Briceño-Hansen en una teoría de campos en el lattice.

Abstract

Lattice QCD (LQCD) offers a non-perturbative scheme that enables the analysis of hadronic systems using computational methods. Most of the hadronic states decay strongly into multiparticle states, i.e. they are resonant states. Aiming to extend the applications of lattice field theories, the Briceño-Hansen formalism establishes a relation between the finite volume matrix elements of external currents, which are computed on the lattice, and the corresponding infinite volume transition amplitudes between two particle states. In nuclear physics, this formalism will allow the analysis of hadronic structures for two particle states using LQCD. This includes resonant states, like glueballs and pentaquarks, as well as bound states, like the deuteron. Since LQCD studies require plenty of time and computational resources, in this thesis we explore the application of the Briceño-Hansen formalism in a model consisting of two coupled Ising models. We observe that it is possible to extract the matrix elements for one-particle states. The following step will be to extract the matrix elements for two-particle states, which will provide all the necessary ingredients for testing the Briceño-Hansen formalism in a lattice field theory for the first time.

Contents

1	Introduction	1
I	Lattice field theories	4
2	Scalar fields on the lattice	5
2.1	Scalar fields in 1+1D Minkowski-type space	5
2.2	Scalar fields in 2D Euclidean lattice	6
2.3	Scaling limit of a $\lambda\phi^4$ theory	7
II	Evaluating a field theory on a lattice	8
3	The Gattringer-Lang model	9
3.1	Two coupled scalar fields	9
3.2	Dispersive representation of the Euclidean correlator	10
3.3	Momentum operators	12
4	Simulation algorithm	13
4.1	Updating the heavy field	14
4.2	Updating the φ field	15
5	Analysis of correlation functions	17
5.1	Setup	17
5.2	One-particle sector	18
5.3	Two-particle sector	20
III	Scattering amplitudes and form factors	26
6	Infinite volume elastic scattering	27
6.1	Irreducible diagrams	27
6.2	The one-loop term	28
6.3	All orders perturbation theory	30
6.4	Implications of the unitarity of the \mathcal{S} -matrix	31
6.5	Lüscher formalism in 1+1D	32

7	Finite-volume matrix elements of scalar currents	35
7.1	Briceño-Hansen formalism in 1+1D	35
7.2	Three-point correlators of one-particle states	36
7.3	Smearred operators	37
7.4	Matrix elements	38
8	Conclusion	41
	Appendix	42
	Appendix A Jackknife statistics	43
A.1	Bins, jackknife ensembles and errors	43
A.2	Observables and covariance	44

CHAPTER 1

Introduction

Around the globe, numerous groups of theoretical nuclear and particle physicists are continuously advancing in the comprehension of the spectrum and structure of hadrons. For the former, the hadronic states are extracted directly from Quantum Chromodynamics (QCD), while for the latter the arrangement of quarks and gluons inside the hadrons is studied. It is expected that, by understanding the spectrum of the theory, as well as its relation to the structure of the states, it could be possible to shed some light on the mechanism that confines quarks and gluons into hadrons, one of the unanswered questions of QCD. This has in part motivated searches of exotic configurations of QCD like glueballs, tetraquarks, pentaquarks, molecules, etc. (see Refs. [Lebed et al., 2017, Guo et al., 2018, Briceño et al., 2016, Chen et al., 2016, Liu, 2014] for recent reviews on these topics).

The determination of the hadronic spectrum from QCD has two major obstacles. First, the non-perturbative nature of QCD at low energies prohibits the use of standard perturbative methods when studying nuclear phenomena. Secondly, the fact that most of the hadrons decay strongly into multi-particle states, characterizing them as resonances. As a consequence, the identification of resonant states requires knowledge of the scattering amplitude of its decay products. Both of these difficulties can be circumvented through the numerical technique known as lattice field theories.

Lattice field theories provide a non-perturbative scheme to study quantum field theories, like QCD, by truncating and discretizing spacetime with imaginary time, i.e. by evaluating field theories in a Euclidean lattice. As we will see later in this thesis, there is a direct relation between two-point correlation functions and the spectrum of the theory. However, truncation of spacetime comes at a cost of losing a rigorous definition of asymptotic states, a necessary prerequisite for defining scattering amplitudes. Therefore, the study of resonances on the lattice is a non-trivial task. As first pointed out by [Lüscher, 1991], there exists a relationship between the finite-volume spectrum of two particles and their infinite volume scattering amplitude. The key point was the construction of non-perturbative relations between finite- and infinite-volume observables. This has proven to be remarkably useful and has since been generalized and successfully implemented for a variety of observables (for a recent review [Briceño et al., 2018]).

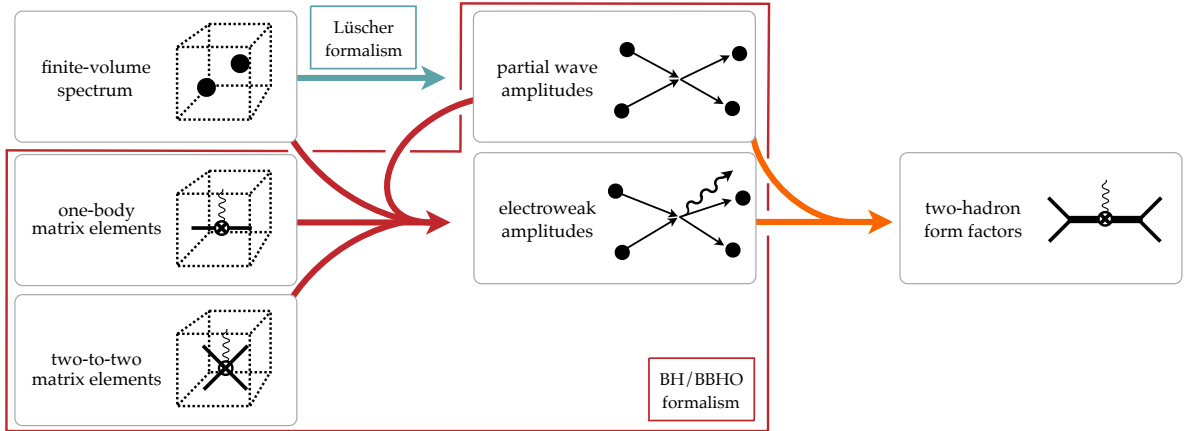


Figure 1.1: This flowchart displays the main components of the Lüscher and Briceño-Hansen formalism for the structure of two-particle states, adapted from [Baroni et al., 2019].

Although the determination of the hadronic spectrum, including resonant states, through Lattice QCD (LQCD) is a valuable piece in the puzzle of the strong interaction, it would be desirable to have access to a broader type of phenomena. In particular, we wish to be able to access their structural information. Just as with stable hadrons, one can access their structure by probing them with external currents. It was proposed in Refs. [Briceño and Hansen, 2016, Baroni et al., 2019] that the structure of resonances and bound states may be determined from transition amplitudes between two-particle states mediated by a single current insertion, and this proposal is the main focus of this work. The Briceño-Hansen formalism, schematically outlined in Figure 1.1, provides a non-perturbative relationship between the finite-volume matrix elements of two-particles and the previously-mentioned amplitudes.

Even though some important formal checks have been carried out [Briceño et al., 2019, Baroni et al., 2019], this formalism has not been implemented in lattice calculation to date. This is because the non-perturbative mapping requires a variety of non-trivial pieces which must be determined in a lattice calculation:

- the finite-volume spectrum of one-particle states,
- the finite-volume spectrum of two-particle states,
- the finite-volume matrix elements of one-particle states,
- the finite-volume matrix elements of two-particle states.

In this work we present results of the first three bullet points for a toy resonant scalar field theory in 1+1D. The primary reason for carrying out this exploratory calculation in a toy scalar field theory is that these are computationally and conceptually far cheaper than their QCD counterparts. Thereby, one can test the formalism and the subsequent analysis with minimal resources. This has motivated previous studies of two-body scattering using this model, first

by [Gattringer and Lang, 1993] in 1+1D, later by [Rummukainen and Gottlieb, 1995] in 3+1D, and more recently by [Guo, 2013], with two coupling channels, and in [Guo and Gasparian, 2018] considering three-body scattering observables.

This work is organized as follows. In Part I, we review the field theory considered here. We start by presenting it as a continuum theory in 1+1D Minkowski-type space and show how it can be discretized in a 2-dimensional Euclidean lattice. In Part II we discuss the toy model used to explore the Lüscher and Briceño-Hansen formalism, which we will refer to as the “Gattringer-Lang model”. First, we review the general properties of the model, which consists of two real scalar fields sharing a coupling channel. Then we present the multi-cluster algorithm implemented by Gattringer and Lang for their study and in the end we reproduce the spectrum of the theory as obtained in [Gattringer and Lang, 1993]. This part emphasizes the relation between the two-point Euclidean correlation functions and the spectrum of the theory. Finally, in Part III we present our results. First we rederive the main results for two-particle scattering of a $\lambda\phi^4$ theory in 1 + 1D Minkowski-type space. Then we review the Lüscher formalism in 1+1D finite volume following the same analysis by [Kim et al., 2005]. At this point the relation between the two-particle spectrum and the scattering phase-shift will be evident. The scattering phase-shift was also obtained in [Gattringer and Lang, 1993]. Finally we discuss the Briceño-Hansen formalism in 1 + 1D and present the matrix elements for one-particle states coupling to a smeared current, an analysis that has not been previously performed for the Gattringer-Lang model. The results presented here are relevant since they provide three out of four necessary pieces for testing the Briceño-Hansen formalism in a lattice field theory.

Part I
Lattice field theories

CHAPTER 2

Scalar fields on the lattice

The Euclidean lattice regularization provides a non-perturbative framework for the evaluation of field theories. Lattice field theories require going from a continuous and infinite volume to a discretized and finite volume, where the field theory can be studied through computer simulations. In this chapter we review the lattice formulation of a scalar field theory following [Gattringer and Lang, 2010]. In particular, we are interested in considering the case of a $\lambda\phi^4$ theory in the so called scaling limit.

2.1 Scalar fields in 1+1D Minkowski-type space

The path integral representation for the correlator of two operators, say \mathcal{O}_1 and \mathcal{O}_2 , in a scalar field theory in 1+1 dimensional Minkowski-type space is given by

$$\langle \hat{\mathcal{O}}_2(x_0) \hat{\mathcal{O}}_1^\dagger(0) \rangle = \frac{\int \mathcal{D}\phi \mathcal{O}_2[\phi(x_0, \cdot)] \mathcal{O}_1^\dagger[\phi(0, \cdot)] e^{iS[\phi]}}{\int \mathcal{D}\phi e^{iS[\phi]}}. \quad (2.1.1)$$

Here x_0 denotes real time and the notation $[\phi(x_0, \cdot)]$ indicates evaluation over all possible classical configurations of the field at the correlation time x_0 . Therefore, the quantities $\mathcal{O}[\phi(x_0, \cdot)]$ represent functionals of the classical field variables rather than operators.

The action of a real scalar field is an integral over space and time of the Lagrangian density

$$S[\phi] = \int dx_0 dx_1 \mathcal{L}(\phi(x_0, x_1), \partial_\mu \phi(x_0, x_1)). \quad (2.1.2)$$

For an interacting potential depending only on $\phi(x)$, the Lagrangian density reads

$$\begin{aligned} \mathcal{L}(\phi(x_0, x_1), \partial_\mu \phi(x_0, x_1)) &= \frac{1}{2} (\partial_\mu \phi)(\partial^\mu \phi) - \frac{m^2}{2} \phi^2 - V(\phi), \\ &= \frac{1}{2} \frac{\partial^2 \phi}{\partial x_0^2} - \frac{1}{2} \frac{\partial^2 \phi}{\partial x_1^2} - \frac{m^2}{2} \phi^2 - V(\phi), \end{aligned} \quad (2.1.3)$$

where we use the convention $g_{\mu\nu} = \text{diag}\{1, -1\}$.

2.2 Scalar fields in 2D Euclidean lattice

First we perform a Wick rotation to imaginary time, $t = ix_0$, so the relative sign between the space and time derivatives in (2.1.3) is removed. Thus we have gone from the Minkowski-type 1+1 dimensional space with metric $g_{\mu\nu} = \text{diag}\{1, -1\}$ (where $\mu, \nu = 0, 1$) to the 2D Euclidean space with metric $g_{\mu\nu} = \text{diag}\{1, 1\} = \delta_{\mu\nu}$ (where $\mu, \nu = 1, 2$). As a result, the action is given by

$$iS[\phi] = - \int dx_1 dt \left\{ \frac{1}{2} \frac{\partial^2 \phi}{\partial t^2} + \frac{1}{2} \frac{\partial^2 \phi}{\partial x_1^2} + \frac{m^2}{2} \phi^2 + V(\phi) \right\}. \quad (2.2.1)$$

This leads us to identify the Euclidean action as

$$S_E[\phi] = \int dx_1 dt \left\{ \frac{1}{2} \frac{\partial^2 \phi}{\partial x_1^2} + \frac{1}{2} \frac{\partial^2 \phi}{\partial t^2} + \frac{m^2}{2} \phi^2 + V(\phi) \right\}, \quad (2.2.2)$$

and the path integral representation of the Euclidean correlator as

$$\langle \hat{\mathcal{O}}_2(t) \hat{\mathcal{O}}_1(0) \rangle_E = \frac{\int \mathcal{D}\phi \mathcal{O}_2[\phi(\cdot, t)] \mathcal{O}_1[\phi(\cdot, 0)] e^{-S_E[\phi]}}{\int \mathcal{D}\phi e^{-S_E[\phi]}}. \quad (2.2.3)$$

Now we introduce the 2D lattice

$$\Lambda \equiv \{n = (n_1, n_2) \mid n_1 = 0, 1, \dots, L-1 \text{ and } n_2 = 0, 1, \dots, T-1\}, \quad (2.2.4)$$

where L and T are the number of sites in the space and time direction, respectively. This way, the fields exist only at the points

$$x = (n_1, n_2), \quad x \in \Lambda. \quad (2.2.5)$$

We consider an isotropic lattice with unit separation between the lattice sites n . Then, the integrals and derivatives can be replaced by the discrete sums and differences

$$\int dx_1 dt \rightarrow \sum_{n_1=0}^{L-1} \sum_{n_2=0}^{T-1} \quad \text{and} \quad \partial_\mu \phi(x) \rightarrow \phi(x + \hat{\mu}) - \phi(x), \quad |\hat{\mu}| = 1. \quad (2.2.6)$$

Here $\hat{\mu}$ denotes a unit vector along either, the space ($\mu = 1$) or time ($\mu = 2$) direction.

Therefore, the Euclidean action on a $L \times T$ lattice reads

$$S_E[\phi] = \sum_{x \in \Lambda} \left\{ \frac{1}{2} \sum_{\mu=1,2} [\phi(x + \hat{\mu}) - \phi(x)]^2 + \frac{m^2}{2} \phi(x)^2 + V(\phi(x)) \right\}, \quad (2.2.7)$$

where $x \in \Lambda$ indicates that the sum is performed over all the lattice sites. We impose periodic boundary conditions by identifying

$$\phi(L, t) = \phi(0, t) \quad \text{and} \quad \phi(x_1, T) = \phi(x_1, 0). \quad (2.2.8)$$

2.3 Scaling limit of a $\lambda\phi^4$ theory

Inserting a potential proportional to ϕ^4 , the Euclidean action (2.2.2) reads

$$S_E[\phi] = \int dx_1 dt \left\{ \frac{1}{2} \frac{\partial^2 \phi}{\partial x_1^2} + \frac{1}{2} \frac{\partial^2 \phi}{\partial t^2} + \frac{m^2}{2} \phi^2 + \frac{\lambda_0}{4!} \phi^4 \right\}, \quad (2.3.1)$$

which taken to the grid becomes

$$S_E[\phi] = \sum_x \left\{ \frac{1}{2} \sum_{\mu} [\phi(x + \hat{\mu}) - \phi(x)]^2 + \frac{m^2}{2} \phi^2(x) + \frac{\lambda_0}{4!} \phi^4(x) \right\}. \quad (2.3.2)$$

By rescaling the field and performing the substitutions

$$\phi(x) = \sqrt{2\kappa} \varphi(x), \quad m^2 = \frac{1 - 2\lambda}{\kappa} - 4, \quad \lambda_0 = \frac{6\lambda}{\kappa^2}, \quad (2.3.3)$$

the Euclidean action can be written as

$$S_E[\varphi] = \sum_x \left\{ -2\kappa \sum_{\mu} \varphi(x + \hat{\mu}) \varphi(x) + \varphi^2(x) + \lambda [\varphi^2(x) - 1]^2 - \lambda \right\}, \quad (2.3.4)$$

where the last term constitutes a constant that can be neglected.

In the limit $\lambda \rightarrow \infty$ at fixed κ , which the literature refers to as the “scaling limit”, only the $\varphi^2(x) = 1$ configurations contribute to the action since the third term would diverge otherwise. Thus, in this limit, the second term becomes yet another constant and the third term is cancelled out, simplifying the Euclidean action to

$$S_E[\phi] = -2\kappa \sum_{x,\mu} \varphi(x + \hat{\mu}) \varphi(x), \quad \varphi(x) = \pm 1. \quad (2.3.5)$$

The form above for the Euclidean action of a $\lambda\phi^4$ theory resembles a well known and highly investigated system in physics. An arrangement of spins $\sigma(x) = \pm 1$ at the sites of the lattice and whose Hamilton function (in absence of an external field) involves interactions between nearest neighbors only, is known as the Ising model. By defining J as the nearest neighbor coupling, the Hamilton function for the Ising model can be written as

$$H = -J \sum_{x,\mu} \sigma(x + \hat{\mu}) \sigma(x), \quad \sigma(x) = \pm 1. \quad (2.3.6)$$

Scaling this by the inverse temperature leads to the Euclidean action (2.3.5).

In general, the properties of the Ising model can be studied statistically through the generation of a large number of spins configurations and the analysis of its correlation functions. In this work, following the analyses performed by [Gattringer and Lang, 1993] and [Guo, 2013] described in the next part, we implement a Swendsen-Wang multicluster algorithm. We then proceed to evaluate and analyze two- and three-point correlation functions for this theory. These steps are described in the subsequent parts.

Part II

Evaluating a field theory on a lattice

CHAPTER 3

The Gattringer-Lang model

In the first part of this thesis we reviewed how a real scalar field can be taken to the Euclidean lattice and that the scaling limit of this field theory under a $\lambda\phi^4$ interaction is the Ising model. Based on the latter, a two-dimensional system with resonant scattering between two scalar fields was proposed by [Gattringer and Lang, 1993]. That model has been generalized to four-dimensional Euclidean lattices [Rummukainen and Gottlieb, 1995] and to include more than two scalar fields [Guo, 2013]. Chapter 4 is dedicated to describe the sampling algorithm. Chapter 5 presents the analysis of two-point correlators in the one- and two-particle sector. In the present chapter we review the general properties of the Gattringer-Lang model (GL model) and introduce the dispersive representation of the two-point Euclidean correlator which, as we will see, is related to the spectrum of the theory.

3.1 Two coupled scalar fields

The 2D GL model consists of two spin fields coupled through a cubic term

$$\begin{aligned} S_E[\varphi, \rho] = & -\kappa_\varphi \sum_{x,\mu} \varphi(x)\varphi(x + \hat{\mu}) - \kappa_\rho \sum_{x,\mu} \rho(x)\rho(x + \hat{\mu}) \\ & + \frac{g}{2} \sum_{x,\mu} \rho(x)\varphi(x) [\varphi(x + \hat{\mu}) + \varphi(x - \hat{\mu})], \end{aligned} \quad (3.1.1)$$

where, compared to equation (2.3.5), the factor of 2 from the Ising models has been absorbed into the hopping parameters κ_φ , κ_ρ , and g is a coupling constant.

In the decoupling limit, $g = 0$, each field behaves as an independent Ising model and thus the mass of each interacting boson can be determined from its corresponding hopping parameter [Itzykson and Drouffe, 1989]

$$m = -\ln(\tanh \kappa) - 2\kappa. \quad (3.1.2)$$

In the coupled case, $g > 0$, the masses of the fields are determined by the parameters κ_φ and κ_ρ as well as the value of the coupling constant.

Provided that the coupling constant g is small, in the scaling limit, the GL model (3.1.1) is expected to resemble the field theory of two real scalar fields under fourth-power self-interactions with a coupling channel

$$S_E[\phi, \eta] = \int d^2x \left\{ \frac{1}{2} \partial_\mu \phi \partial_\mu \phi + \frac{m_\phi^2}{2} \phi^2 + \frac{\lambda_\phi}{4!} \phi^4 \right\} + \int d^2x \left\{ \frac{1}{2} \partial_\mu \eta \partial_\mu \eta + \frac{m_\eta^2}{2} \eta^2 + \frac{\lambda_\eta}{4!} \eta^4 \right\} + G \int d^2x \eta \phi^2. \quad (3.1.3)$$

Here, according to the substitutions (2.3.3), ϕ and η represent the rescaled fields corresponding to φ and ρ , respectively, and the rescaled coupling constant G is proportional to g

$$G \sim g \frac{1}{\kappa_\varphi \sqrt{\kappa_\rho}}. \quad (3.1.4)$$

The coupling term in (3.1.1) and (3.1.3) arranges for the interaction between both types of fields. By adjusting the hopping parameters, the corresponding masses of the rescaled fields φ and ρ can be fixed. As we will see in Chapter 5, the mass of the ρ and φ fields can be chosen in such a way that

$$2m_\varphi < m_\rho < 4m_\varphi. \quad (3.1.5)$$

By considering the range of energies $2m_\varphi < E < 4m_\varphi$, we necessarily have elastic scattering since the model does not allow for processes where an even number of particles couple to an odd number of particles (e.g. $2\varphi \rightarrow 3\varphi$). Furthermore, since we have tuned the masses of the theory to satisfy (3.1.5), we assure that we obtain a resonant amplitude in the elastic two-particle φ scattering amplitude.

In Chapter 6 we will see that (3.1.5) sets the condition for elastic scattering since the mass of the heavier field (ρ) lies within the range of energies where two particles of the lighter field (φ) can go on-shell. Then, when $g \neq 0$, the coupling term gives rise to a resonant behavior for the heavy field in a two-particle channel $\rho \rightarrow \varphi\varphi$. In what follows, we restrict our attention to kinematics where states with more than two particles cannot go on-shell.

3.2 Dispersive representation of the Euclidean correlator

In order to derive the dispersive representation of the Euclidean correlator, we begin by reviewing the normalization of the eigenstates for the Hamilton operator, which pose a complete basis. Within a one-dimensional infinite volume the standard relativistic normalization for single-particle states is given by

$$\langle p|q \rangle = 2\pi 2E(p) \delta(q - p). \quad (3.2.1)$$

Moving to a one-dimensional finite volume of size L , momentum is quantized so the Dirac δ in (3.2.1) is changed for a Kronecker δ . In what follows, it is convenient to introduce an integer ℓ

that enumerates all possible discrete states in a finite volume. With this, we define finite-volume states to be normalized to

$$\langle \ell; p_n | \ell'; p_{n'} \rangle = 2E_\ell(p_n) \delta_{\ell\ell'} L \delta_{nn'}, \quad (3.2.2)$$

which allows us to write the identity in terms of a sum discrete states with fixed momentum

$$\mathbb{1} = \sum_{\ell=0}^{\infty} \frac{1}{2LE_\ell(p_n)} |\ell; p_n\rangle \langle \ell; p_n|, \quad p_n = \frac{2\pi n}{L}, \quad (3.2.3)$$

where $n = L/2, L/2 - 1, \dots, -L/2 + 1$. This is the completeness relation in a one-dimensional finite volume.

Working in a Hilbert space with imaginary time t of finite extent T , for any two operators the Euclidean correlator is

$$\begin{aligned} \langle \hat{\mathcal{O}}_2(t) \hat{\mathcal{O}}_1^\dagger(0) \rangle_T &\equiv \frac{1}{Z_T} \text{tr} \{ e^{-T\hat{H}} \hat{\mathcal{O}}_2(t) \hat{\mathcal{O}}_1^\dagger(0) \}, & Z_T &\equiv \text{tr} \{ e^{-T\hat{H}} \}, \\ &= \frac{\sum_\ell \langle \ell | e^{-T\hat{H}} \hat{\mathcal{O}}_2(t) \hat{\mathcal{O}}_1^\dagger(0) | \ell \rangle}{\sum_\ell \langle \ell | e^{-T\hat{H}} | \ell \rangle}. \end{aligned} \quad (3.2.4)$$

Now, making use of the completeness relation (3.2.3) and the time evolution of Heisenberg operators in Euclidean space

$$\hat{\mathcal{O}}(t) = e^{t\hat{H}} \hat{\mathcal{O}}(0) e^{-t\hat{H}}, \quad (3.2.5)$$

the correlator can be expanded as

$$\begin{aligned} \langle \hat{\mathcal{O}}_2(t) \hat{\mathcal{O}}_1^\dagger(0) \rangle_T &= \frac{\sum_{\ell, \ell'} \frac{1}{2LE_{\ell'}} e^{-(T-t)E_\ell} \langle \ell | \hat{\mathcal{O}}_2 | \ell' \rangle e^{-tE_{\ell'}} \langle \ell' | \hat{\mathcal{O}}_1^\dagger | \ell \rangle}{\sum_\ell e^{-TE_\ell}} \\ &= \frac{\sum_{\ell, \ell'} \frac{1}{2LE_{\ell'}} e^{-(T-t)\Delta E_\ell} e^{-t\Delta E_{\ell'}} \langle \ell | \hat{\mathcal{O}}_2 | \ell' \rangle \langle \ell' | \hat{\mathcal{O}}_1^\dagger | \ell \rangle}{1 + e^{-T\Delta E_1} + \dots}, \end{aligned} \quad (3.2.6)$$

where, in the last step, we have factorized the ground state weight factor $\exp\{-TE_0\}$ from all the terms in both the numerator and the denominator, so $\Delta E_\ell = E_\ell - E_0$. In the limit $T \rightarrow \infty$, all the terms with $\ell \neq 0$ vanish and we are left with the expectation values of operators evaluated with respect of the vacuum only

$$\lim_{T \rightarrow \infty} \langle \hat{\mathcal{O}}_2(t) \hat{\mathcal{O}}_1^\dagger(0) \rangle_T = \sum_{\ell' > 0} \frac{1}{2LE_{\ell'}} e^{-tE_{\ell'}} \langle 0 | \hat{\mathcal{O}}_2 | \ell' \rangle \langle \ell' | \hat{\mathcal{O}}_1^\dagger | 0 \rangle, \quad (3.2.7)$$

where we have set $E_0 = 0$.

In summary, the energy eigenstates constitute a normalized basis allowing us to study Euclidean correlators on the lattice. In this way, the two-point correlation function (3.2.4) can be expressed as the spectral decomposition (3.2.7) in the limit when the extension of the Euclidean imaginary time T goes to infinity. Then, since the Euclidean correlator displays a direct relation with the spectrum of the theory, we can exploit this fact with the right choice of operators to be evaluated in the two-point function.

3.3 Momentum operators

In general, the operators appearing in the Euclidean correlator (3.2.7) can be built from field operators defined on the lattice sites or, through a Fourier transform from their corresponding states with definite momentum. In a finite volume of size L the momentum p of a particle is discretized and the states with definite momentum are given by

$$\tilde{\varphi}(n, t) = \sum_{x_1} \varphi(x_1, t) e^{i x_1 p_n}. \quad (3.3.1)$$

Here the sum is carried out over all the spatial positions of the lattice at time-slice t . The corresponding inverse transform reads

$$\varphi(x_1, t) = \frac{1}{L} \sum_n \tilde{\varphi}(n, t) e^{-i x_1 p_n}. \quad (3.3.2)$$

Operators (3.3.1) and (3.3.2) correspond to the one-particle states of the theory. Two-particle states with total momentum zero can be built out of single particle operators with relative momentum $2p_n$

$$\tilde{\varphi}_n^{(2)}(0, t) = \tilde{\varphi}(n, t) \tilde{\varphi}(-n, t) = \sum_{x_1, y_1 \in \Lambda_t} \varphi(x_1, t) \varphi(y_1, t) e^{i(x_1 - y_1) p_n}. \quad (3.3.3)$$

However, due to the condition of elastic scattering (3.1.5) and the coupling channel $\rho \rightarrow \varphi\varphi$, these operators can also mix with the interpolating operators of the ρ field with zero momentum

$$\tilde{\rho}(0, t) = \sum_{x_1 \in \Lambda_t} \rho(x_1, t), \quad (3.3.4)$$

since it shares the quantum numbers of $\tilde{\varphi}^{(2)}$. In fact, it is empirically well known from lattice calculations, that in order to reliably extract the spectrum of resonant systems it is necessary to accommodate the mixing of these operators and diagonalize correlation functions appropriately. The standard technique used for effectively diagonalizing correlation functions involves solving the generalized eigenvalue problem (GEVP), which we review in Section 5.3 (see [Briceño et al., 2018] for a pedagogical introduction).

In Chapter 5 we will show how the spectrum of the one- and two-particle sector of the theory can be constructed by evaluating the two-point correlation functions (3.2.4) of the corresponding momentum operators in a large ensemble of field configurations. The generating algorithm for the field configurations, presented in the next chapter, enables the extraction of the spectrum.

CHAPTER 4

Simulation algorithm

In order to evaluate Euclidean correlators on the lattice, we need a large number of configurations for the φ and ρ fields. A modified version of the Swendsen-Wang (SW) algorithm was adapted by [Gattringer and Lang, 1993], which we review here. In this chapter we address their generating algorithm. A typical configuration of the fields can be imaged as the one displayed on Figure 4.1, where red and blue can represent -1 and $+1$ valued fields, respectively. As we will see, each field is updated alternately following a SW routine adapted to take into account the coupling g in the Euclidean action (3.1.1). In Chapter 5 we will see that, for the selected values of κ_ρ and κ_φ , the mass of the ρ field is larger than the mass of the φ field. Therefore, we refer to the former as the heavy field and the latter as the light field.

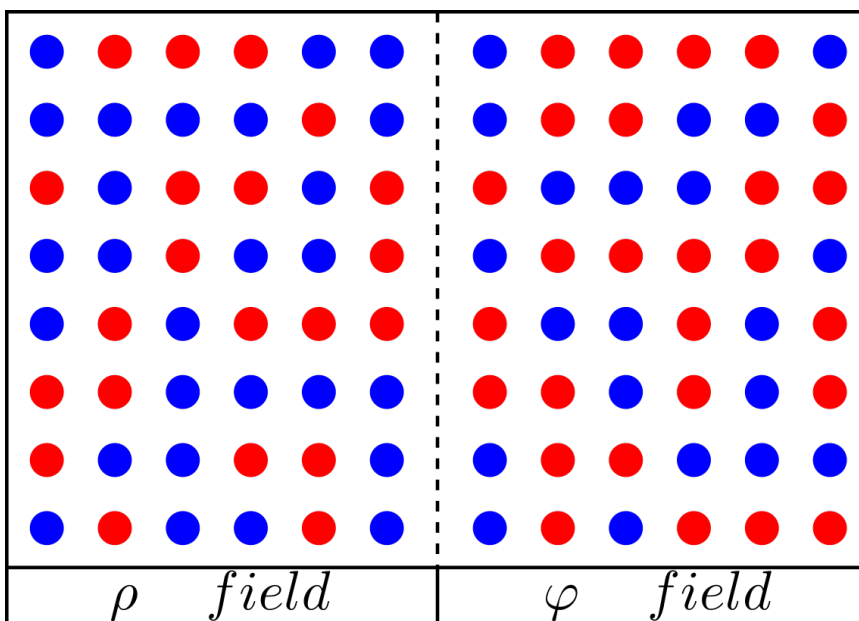


Figure 4.1: A possible initial configuration of the fields.

4.1 Updating the heavy field

As a starting point we consider any given configuration of the ρ and φ fields, e.g. Figure 4.1. From here, each Ising model is updated alternately. This means that when one of the fields is being updated (for example $\rho \rightarrow \rho'$) the other field remains the same (thus $\varphi \rightarrow \varphi$); then the former field remains the same ($\rho' \rightarrow \rho'$) while the latter is updated ($\varphi \rightarrow \varphi'$). Below, we describe how the configurations of the ρ and φ fields are generated.

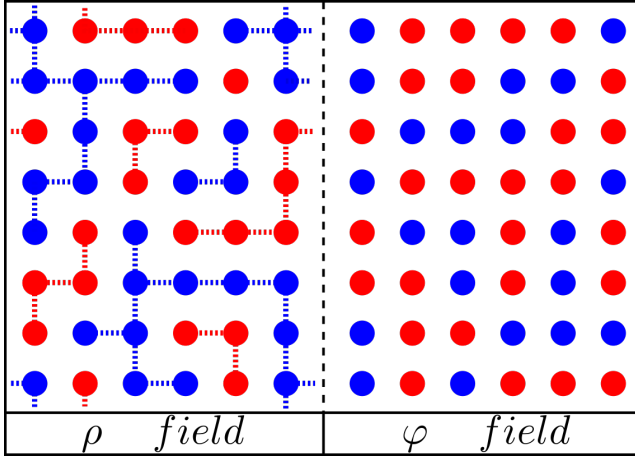


Figure 4.2: Possible bonds between neighboring spins with equal sign of the heavy field.

First, a bond can exist between any two neighboring spins with equal sign. In Figure 4.2 the dashed lines show every possible bond in the initial configuration of Figure 4.1. A bond between the spin at site x and its neighbor in the $\hat{\mu}$ direction is set with probability¹

$$P_{\text{bond}}(\rho; x, \mu) = 1 - e^{-2\kappa\rho}. \quad (4.1.1)$$

It is important to notice that, since the lattice has periodic boundary conditions, bonds can be established across the boundaries.

Second, a cluster is formed by all spins connected by bonds, as shown in Figure 4.3. After all bonds of the configuration have been established and the clusters have been formed, the sign of all the spins within a given cluster are flipped with probability

$$P_{\text{flip}}(\rho, \varphi; C) = \frac{1}{1 + e^{-2\alpha(C)}}. \quad (4.1.2)$$

Here C represents any cluster of the ρ configuration and $\alpha(C)$ is a sum of the three-point term evaluated over all the sites in the cluster

$$\alpha(C) = \frac{g}{2} \sum_{x \in C} \sum_{\mu=1,2} \rho(x) \varphi(x) [\varphi(x - \hat{\mu}) + \varphi(x + \hat{\mu})]. \quad (4.1.3)$$

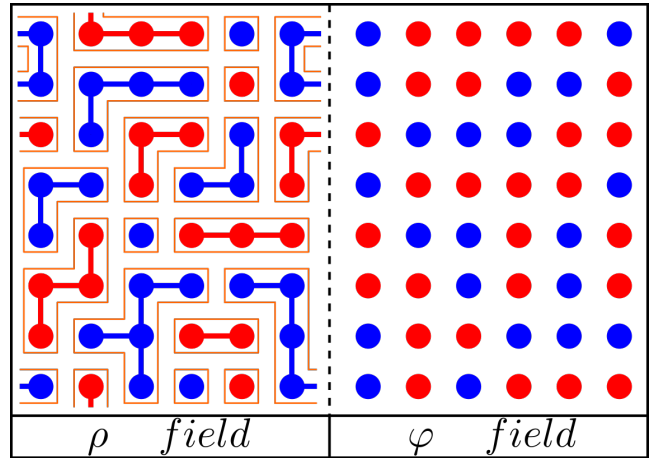


Figure 4.3: Clusters resulting from the activated bonds of the ρ field.

¹In general terms, the exponent represents the change in the action contribution of two neighboring spins when the sign of either of them is flipped, see [Swendsen and Wang, 1987] for details.

This can be seen as the background of the φ field during the process of generating a new configuration for the ρ field. This behavior is displayed in Figure 4.4 where the yellow area represents a cluster of the ρ field and the green area represents the spins of the φ field playing a role on whether or not the cluster is flipped. Finally, after the clusters have been flipped according to probability (4.1.2), a new configuration of the ρ field has been generated, see Figure 4.5.

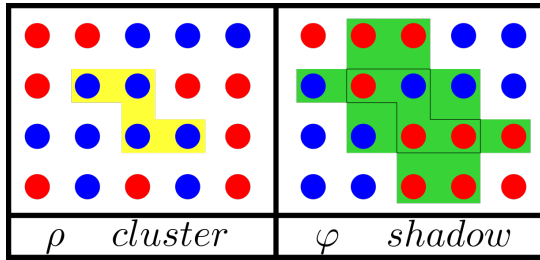


Figure 4.4: Representation of the relation between the fields while updating a cluster of the heavy field.

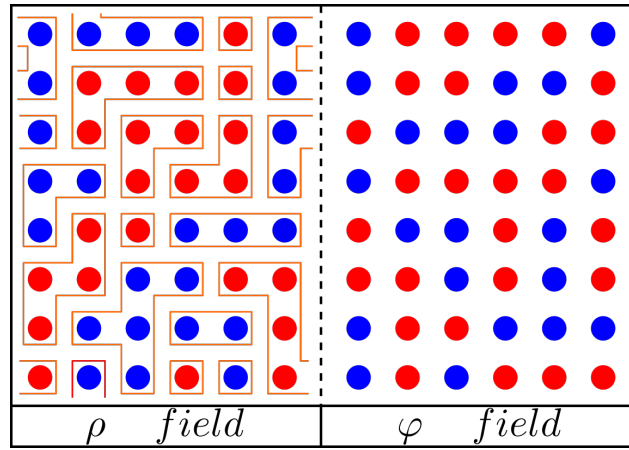


Figure 4.5: New configuration of the heavy field, the light field remains unchanged.

4.2 Updating the φ field

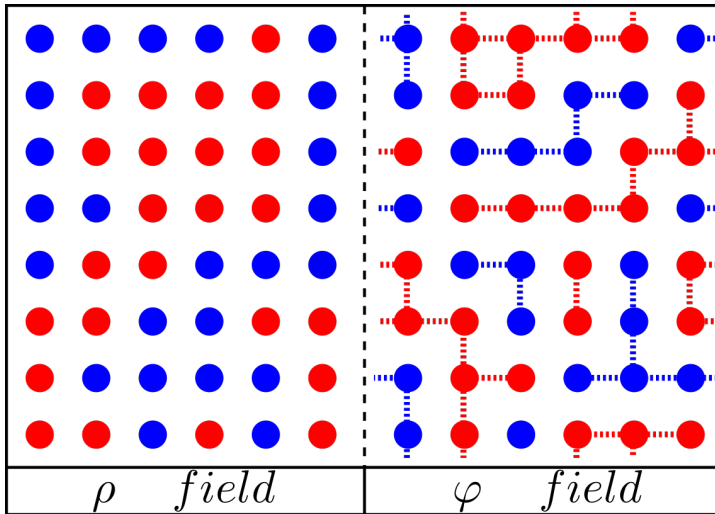


Figure 4.6: Possible bonds between neighboring spins with equal sign of the light field.

After having modified the ρ field, now we turn to the φ field. Again, bonds are possible between equally signed neighboring spins of the configuration, see Figure 4.6. In this case, the bonds are set with probability

$$P_{\text{bond}}(\varphi; x, \mu) = 1 - e^{-2\omega(x, \mu)}, \quad (4.2.1)$$

where

$$\omega(x, \mu) = \kappa_\varphi - \frac{g}{2} [\rho(x) + \rho(x + \hat{\mu})].$$

Notice that now the ρ field influences the way bonds are formed within the φ field, see Figure 4.7.

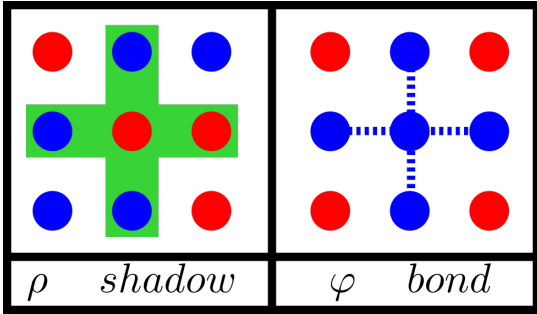


Figure 4.7: Influence of the ρ field on the φ bonds.

The clusters formed by the activated bonds (Figure 4.8) are simply flipped with probability

$$P_{\text{flip}}(\varphi) = \frac{1}{2}. \quad (4.2.2)$$

Finally, after the clusters of the φ field have been updated, a new configuration of the GL model has been generated, see Figure 4.9. Our code for the simulation algorithm has been written in C++ and can be generalized to consider a larger number of fields.

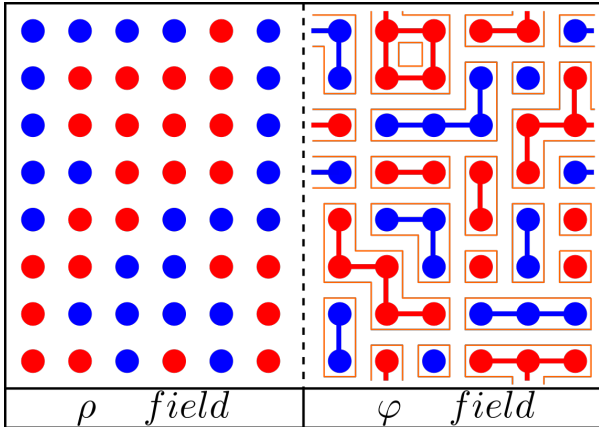


Figure 4.8: Cluster formation.

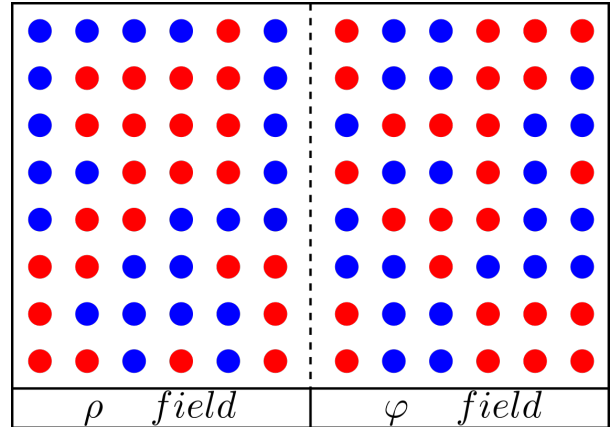


Figure 4.9: New configuration of the model.

Throughout our simulations we work with a lattice of size $L \times T$, where the spatial length ranges from $L = 12$ to $L = 60$ and the time extension is kept fixed at $T = 100$. The cluster algorithm was used to generate 10^6 configurations for each case. However, these configurations are not taken one after another but separated by 20 multi-cluster updates in order to diminish autocorrelation between measurements. We thermalize the system with 10^6 multi-cluster updates before starting to save the configurations. The Euclidean correlators can then be evaluated following the methods discussed in the next chapter.

CHAPTER 5

Analysis of correlation functions

In previous chapters we reviewed the two-point Euclidean correlation function (3.2.7) and the sampling algorithm for the GL model. Provided with a large number of configurations, it is possible to study two-point functions of states with definite momentum, see Section 3.3. In this chapter we describe our algorithm for evaluating the correlators of the one- and two-particle sector and, ultimately, to obtain the spectrum of the GL model. These methods have been applied analogously to other lattice field theories where different types of operators are evaluated on the grid [Lüscher and Wolff, 1990, Dudek et al., 2008]. Our analysis procedure has two parts: first the measurement of the correlators through large number of field configurations and then the fitting routine to extract the energy levels. The former was implemented using C++ while the latter was performed in Python2.7.

5.1 Setup

In [Gattringer and Lang, 1993] three scenarios for the model (3.1.1) are considered. For our study, the following combinations of parameters are useful since they enable a comparison between a resonant and a non-resonant scattering, which is shown in Section 5.3. The values in Table 5.1 were established by Gattringer and Lang so that the φ particle and the ρ particle have masses of approximately 0.2 and 0.5 in lattice units, respectively. Reproducing cases I and II, as studied in [Gattringer and Lang, 1993], allows us to test our algorithms.

Case	I	II
g	0.	0.02
κ_φ	0.3948	0.3897
κ_ρ	0.3268	0.3323

Table 5.1: Coupling constant and hopping parameters for two scenarios. Cases I and II corresponds to non-resonant and resonant scattering, respectively.

5.2 One-particle sector

For the φ field, the Euclidean correlator of one-particle states with momentum p_n is given by the expectation value in the vacuum for the corresponding momentum operators (3.3.1) evaluated at a final time t and initial time set to zero

$$\begin{aligned} C_n(t) &= \langle \Omega | \hat{\varphi}(n, t) \hat{\varphi}^\dagger(n, 0) | \Omega \rangle \\ &= \sum_{\ell} \frac{e^{-E_{\ell}(p_n)t}}{2LE_{\ell}(p_n)} \langle \Omega | \hat{\varphi}(n, 0) | \ell; p_n \rangle \langle \ell; p_n | \hat{\varphi}^\dagger(n, 0) | \Omega \rangle, \end{aligned} \quad (5.2.1)$$

where we have changed the vacuum to be represented by $|\Omega\rangle$, thus representing the empty space, in order to distinguish it from the ground state of the one-particle states $|0; p_n\rangle$, representing the existence of a single particle in its lowest energy state. Due to the $\lambda\phi^4$ interaction, there is an infinite number of states sharing the quantum numbers of a single φ particle, with $\tilde{\varphi}(n, t)$ denoting the operator that interpolates the lowest-lying state.

It is insightful to split the spectral decomposition of the correlator into

$$\begin{aligned} C_n(t) &= \frac{\mathcal{Z}_n^{(0)*} \mathcal{Z}_n^{(0)}}{2LE_0(p_n)} e^{-E_0(p_n)t} + \sum_{\ell \geq 1} \frac{\mathcal{Z}_n^{(\ell)*} \mathcal{Z}_n^{(\ell)}}{2LE_{\ell}(p_n)} e^{-E_{\ell}(p_n)t} \\ &= \frac{|\mathcal{Z}_n^{(0)}|^2}{2LE_0(p_n)} e^{-E_0(p_n)t} [1 + \mathcal{O}(e^{-\Delta E(p_n)t})], \end{aligned} \quad (5.2.2)$$

with $\mathcal{Z}_n^{(\ell)} = \langle \ell; p_n | \hat{\varphi}^\dagger(p_n, 0) | \Omega \rangle$, where we have factored out the contribution of the ground state from those coming from the excited states. Thus, the energy gap $\Delta E(p_n)$ represents the smallest of the differences between the ground state E_0 and the excited states $E_{\ell > 0}$ with momentum p_n . The energy gaps between the excited states and the ground state are positive, so the contributions from excited states are expected to be negligible at large correlation times. We will use this property in our advantage while analyzing the correlation functions.

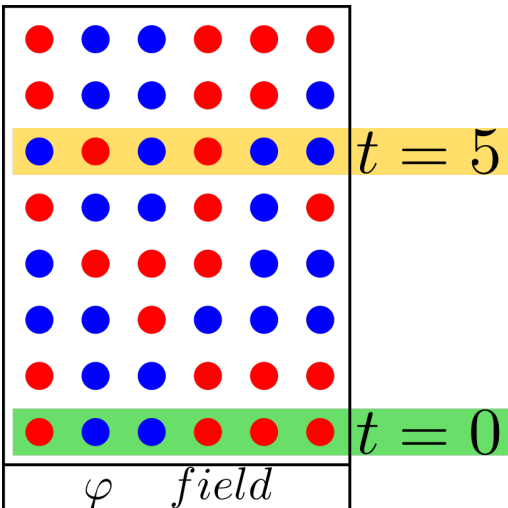


Figure 5.1: A φ sample configuration.

The following example illustrates how the simplest one-particle correlator is evaluated on the lattice for a given configuration and a single correlation time. That process is repeated for all the considered values of momenta and all the available correlation times for each configuration of our generated ensemble.

Example 5.1. For the configuration shown in Figure 5.1 the value of the correlator is given by the product of momentum operators evaluated on the grid. For $n = 0$ and $t = 5$ we have

$$\begin{aligned} C_0(5) &= \tilde{\varphi}(0, 5) \tilde{\varphi}(0, 0), \\ &= (2)(-2) = -4. \end{aligned}$$

Based on a large number, M , of configurations, we can generate an ensemble of correlators for each value of the momentum p_n and correlation time t . We represent these lists of values as

$$\{C_n(t)\}_M = \{\tilde{\varphi}(n,t)\tilde{\varphi}(-n,0)\}_M.$$

Throughout our analysis we worked with $M = 10^6$. To further simplify the analysis, first we bin the results to ensembles of a lesser number of elements $N \ll M$. The resulting ensembles of N elements are analyzed using the jackknife resampling method (see Appendix A). This two-step procedure can be summarized as

$$\{C_n(t)\}_M \xrightarrow{\text{binning}} \{C_n(t)\}_N \xrightarrow{\text{jackknife}} \{C_n(t)\}_N^{JK}.$$

For convenience, we refer to the final ensembles as the “*JK-ensembles*”.

The two-point correlation function of single particle states is constructed from the corresponding JK-ensembles. Figure 5.2 shows the Euclidean correlators extracted from an $L = 60$ lattice for n from 0 to 5. The plot also displays fitted exponentials of the form

$$C_n^{\text{fit}}(t) = \mathcal{A}_n e^{-E_n t}. \quad (5.2.3)$$

Comparing (5.2.3) with (5.2.2), we can identify

$$\mathcal{A}_n \rightarrow \frac{\mathcal{Z}_n^{(0)*} \mathcal{Z}_n^{(0)}}{2LE_0(p_n)} \quad \text{and} \quad E_n \rightarrow E_0(p_n). \quad (5.2.4)$$

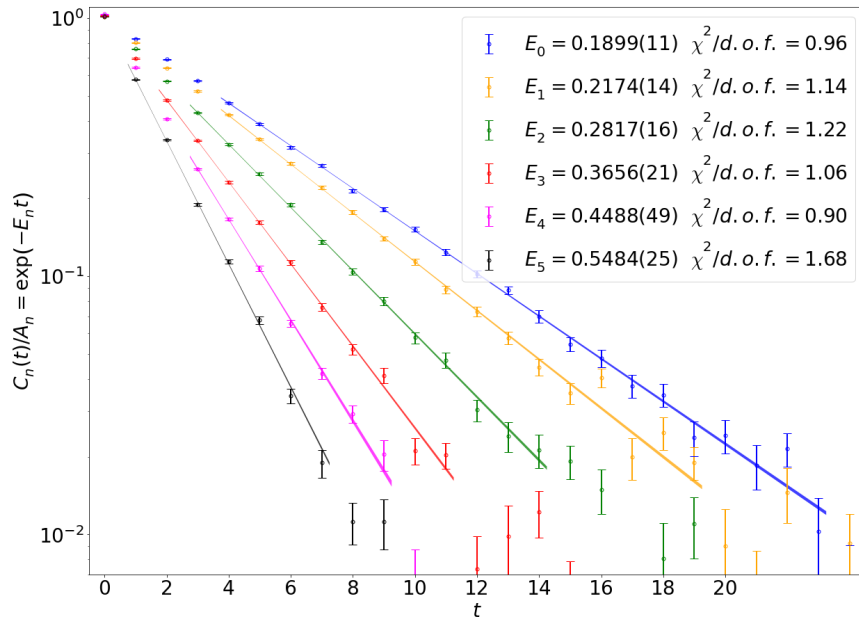


Figure 5.2: Correlators obtained from a 100×60 lattice in the decoupled scenario $g = 0$ (Case I in Table 5.1).

5.3 Two-particle sector

First of all, for the two-particle states the quantum number of momenta is set to zero. In the decoupled case, $g = 0$, the ρ state does not interact with the two-particle φ states. Therefore, in this case, the energy eigenstates of the two-particle sector can be represented as superpositions of momentum eigenstates of two φ particles with total momenta equal to zero but relative momenta $2p_n$. Additionally, due to the elastic scattering condition (3.1.5), the ρ particle exists as a stable state in the same region of energies.

For the coupled case, accessing two-particle states is notoriously more challenging [Briceño et al., 2018]. First, the gap between states is increasingly small. Second, the relative momentum between two particles is not a fixed quantity. Instead, as we will see in Section 6.5, this is fixed by the dynamics of the system, which is exactly what one wishes to determine from lattice calculations. As a result, the optimal interpolating operator for a given ground state is not known. Lastly, as is the case in the GL model, two-particle φ operators can mix strongly with the ρ interpolating operators.

A practical solution to this problem was proposed in [Lüscher and Wolff, 1990], which we follow. The idea is to construct a base of interpolating operators, evaluate all possible correlations between them, and diagonalize the correlation matrix in this basis. This has proven to be successful in fairly complicated resonant and non-resonant systems [Briceño et al., 2018]. In the following example we illustrate how the cross-correlator between the ρ state and a two-particle φ state is evaluated on a given configuration.

Example 5.2: Figure 5.3 shows a sample configuration of the GL model where we can evaluate crossed correlation functions. Let us consider the case when the ρ field couples to a two-particle φ state with zero relative momentum. Their cross-correlator is

$$C_{\varphi_0\rho}(t) = \tilde{\varphi}_0^{(2)}(0, 6)\tilde{\rho}^\dagger(0, 0).$$

For correlation time $t = 6$, the evaluation of the correlator on the given configuration yields the value

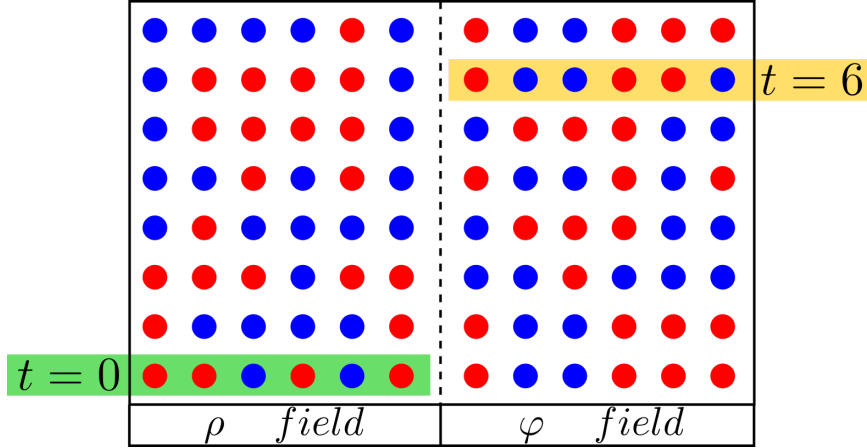
$$C_{\varphi_0\rho}(6) = \tilde{\rho}(0, 6)\tilde{\varphi}_0^{(2)\dagger}(0, 0) = (-2)(0) = 0.$$

To eliminate disconnected contributions to the correlation functions, we take the connected correlation function by subtracting [Forcrand et al., 2004]

$$C_{ij}^{\text{conn}}(t) = C_{ij}^{JK}(t) - C_{ij}^{JK}(t + 1).$$

Thus, from a JK-ensemble of Euclidean correlators we obtain a JK-ensemble of connected correlators

$$\{C_{ij}(t)\}_N^{JK} \longrightarrow \{C_{ij}^{\text{conn}}(t)\}_N^{JK}.$$

Figure 5.3: Sample configuration of the model on a 6×8 lattice.

More explicitly, for the k -th field configuration in the JK-ensemble we define the correlation matrices as

$$C(0, t)^{(k)} = \begin{pmatrix} C_{\rho\rho}(0, t)^{(k)} & C_{\rho\varphi_0}(0, t)^{(k)} & C_{\rho\varphi_1}(0, t)^{(k)} & \dots \\ C_{\varphi_0\rho}(0, t)^{(k)} & C_{\varphi_0\varphi_0}(0, t)^{(k)} & C_{\varphi_0\varphi_1}(0, t)^{(k)} & \dots \\ C_{\varphi_1\rho}(0, t)^{(k)} & C_{\varphi_1\varphi_0}(0, t)^{(k)} & C_{\varphi_1\varphi_1}(0, t)^{(k)} & \dots \\ \vdots & \vdots & \vdots & \ddots \end{pmatrix}. \quad (5.3.1)$$

In principle, since in the continuum limit there is an infinite number of momentum states available, the correlation matrix is infinite in size. By discretizing spacetime, one has introduced an ultra-violet cutoff and consequently limited the number of states. However, this number is far more than one can in practice constrain from any correlation function. The number of states is primarily limited by the size of the interpolating basis used. This can be illustrated by reviewing the spectral decomposition of the Euclidean correlator (3.2.7)

$$\begin{aligned} \langle \hat{\mathcal{O}}_2(t) \hat{\mathcal{O}}_1^\dagger(0) \rangle &= \sum_{\ell} \frac{Z_2^{\ell*} Z_1^{\ell}}{2E_{\ell}} e^{-E_{\ell}t} \\ &= \left[\sum_{\ell=0}^A + \sum_{\ell=A+1}^r + \sum_{\ell=r+1}^{\infty} \right] \frac{Z_2^{\ell*} Z_1^{\ell}}{2E_{\ell}} e^{-E_{\ell}t}. \end{aligned} \quad (5.3.2)$$

In this expression it is assumed that the time extent of the lattice is large enough to be considered infinite and that the energy values are ordered in such a way that $E_0 < E_1 < E_2 < \dots$. The sums within the square brackets have been split into three contributions

1. The states with energies ranging from E_0 to E_A , whose values are within the elastic scattering regime $2m_{\varphi} < E_{\ell} < 4m_{\varphi}$.
2. The states with energies ranging from E_{A+1} to E_r , where $|r\rangle$ would represent the state with the highest energy available on a given lattice.
3. The remaining inaccessible states of the model, with $E_r < E_{\ell \geq r+1}$.

For our analysis we considered up to 6 operators from the two-particle sector, see Section 3.3. These include

$$\begin{aligned}\tilde{\rho}(0, t) &= \sum_{x_1} \rho(x_1, t), & \tilde{\varphi}^{(2)}(0, t) &= \sum_{x_1, y_1} \varphi(x_1, t) \varphi(y_1, t), \\ \tilde{\varphi}^{(2)}(1, t) &= \sum_{x_1, y_1} \varphi(x_1, t) \varphi(y_1, t) e^{i(x_1 - y_1)p_1}, & \tilde{\varphi}^{(2)}(2, t) &= \sum_{x_1, y_1} \varphi(x_1, t) \varphi(y_1, t) e^{i(x_1 - y_1)p_2}, \\ \tilde{\varphi}^{(2)}(3, t) &= \sum_{x_1, y_1} \varphi(x_1, t) \varphi(y_1, t) e^{i(x_1 - y_1)p_3}, & \tilde{\varphi}^{(2)}(4, t) &= \sum_{x_1, y_1} \varphi(x_1, t) \varphi(y_1, t) e^{i(x_1 - y_1)p_4}.\end{aligned}$$

Thus, we work with the basis

$$\left\{ \tilde{\rho}_0, \tilde{\varphi}_0^{(2)}, \tilde{\varphi}_1^{(2)}, \tilde{\varphi}_2^{(2)}, \tilde{\varphi}_3^{(2)}, \tilde{\varphi}_4^{(2)} \right\}, \quad (5.3.3)$$

so have correlation matrices of size 6×6 .

A Lemma by [Lüscher and Wolff, 1990] states that, provided that the eigenvalues λ_ℓ of the correlation matrix are ordered such that $\lambda_0 \geq \lambda_1 \geq \dots \geq \lambda_r$, then as $t \rightarrow \infty$ the eigenvalues have the form

$$\lambda_\ell(t) = C_\ell e^{-E_\ell t} [1 + \mathcal{O}(e^{-|\Delta E_\ell|t})], \quad C_\ell > 0, \quad (5.3.4)$$

for all $\ell \in [0, A]$. Here ΔE_ℓ represents the smallest of the differences between E_ℓ and other eigenenergies.

From the functional form of the eigenvalues, a naive way to find the energy levels of the two-particle sector would be by solving the standard eigenvalue problem

$$C(t) \vec{u}_\ell(t) = \lambda_\ell(t) \vec{u}_\ell(t). \quad (5.3.5)$$

However, the correction in (5.3.4) may not be negligible due to the noise at large correlation times. One way to circumvent this obstacle is to consider the generalized eigenvalue problem (GEVP)

$$C(t) \vec{v}_\ell(t) = \lambda_\ell(t, t_0) C(t_0) \vec{v}_\ell(t), \quad \lambda(t, t_0) = e^{-E_\ell(t-t_0)} [1 + \mathcal{O}(e^{-|\Delta E_\ell|(t-t_0)})], \quad (5.3.6)$$

where $t > t_0$ and $C(t_0)$ represents a metric that arises by choosing a reference time t_0 with the property that the generalized eigenvectors are orthonormal

$$\vec{v}_\alpha(t)^\dagger C(t_0) \vec{v}_\beta(t) = \delta_{\alpha\beta}, \quad (5.3.7)$$

or equivalently

$$V^\dagger(t) C(t_0) V(t) = I, \quad (5.3.8)$$

with $V(t)$ representing the eigenvector matrix.

The GEVP analysis is highly exploited in lattice studies and has a well established and documented solution procedure, see e.g. [Dudek et al., 2008, Gattringer and Lang, 2010]. In the GEVP, the eigenvectors are enforced to be orthogonal on the reference metric, provided that $C(t)$ is saturated by the lowest energy states. This occurs at late reference times t where the higher excited states have decayed. Then, through a Cholesky decomposition [Dudek et al., 2008], the GEVP can be transformed into another standard eigenvalue problem of the form

$$L(t_0)^{-1}C(t)L^\dagger(t_0)^{-1}\vec{w}_\ell(t, t_0) = \lambda_\ell(t, t_0)\vec{w}_\ell(t, t_0), \quad \text{with} \quad L(t_0)L^\dagger(t_0) = C(t_0). \quad (5.3.9)$$

The eigenvalues above have the same form as in (5.3.6) and its eigenvectors are given by

$$\vec{w}_\ell(t, t_0) = L^\dagger(t_0)\vec{v}_\ell(t). \quad (5.3.10)$$

Thus, it is straightforward to recover the generalized eigenvectors \vec{v}_ℓ , whose components indicate the optimal combination of the basis (5.3.3) resembling the energy eigenstates.

By fixing the reference time t_0 and solving the eigenvalue problem posed in (5.3.9) for a range of times $t_0 < t < t^{\max}$, we acquire knowledge of the time-evolution for the proper values of the model, also known as the principal correlators. All the eigenenergies can then be fitted simultaneously by minimizing the quantity

$$\chi^2(E_0, \dots, E_{\ell^{\max}}) = \sum_{\ell, \ell'}^{\ell^{\max}} \sum_{t, t'=t_0+1}^{t^{\max}} \frac{[f(E_\ell, t) - \lambda_\ell(t, t_0)][f(E_{\ell'}, t') - \lambda_{\ell'}(t', t_0)]}{\Delta(\ell, t; \ell', t')}, \quad (5.3.11)$$

where the principal correlators λ_ℓ have been extracted by solving (5.3.9) N times for each correlation time. Δ is the correlation matrix computed through JK-statistics, and the parametrizing function is

$$f(E_n, t) = e^{-E_n(t-t_0)}. \quad (5.3.12)$$

In this two-particle scenario the spectrum reveals one of the characteristic marks of a resonant scattering: as a function of the lattice length, L , in the decoupled limit, the energy levels can cross in certain regions coinciding with the mass of the heavier field while, in the coupled case, such level-crossing is avoided. This behavior can be observed in Figure 5.5, corresponding to $g = 0$, and Figure 5.6, corresponding to $g = 0.02$. The fitted principal correlators for the coupled case are depicted in Figure ???. The two-particle spectrum ultimately gives us access to the resonance parameters through the phase-shift. This will be reviewed in the next part, along with a review of the Lüscher finite-volume formalism.

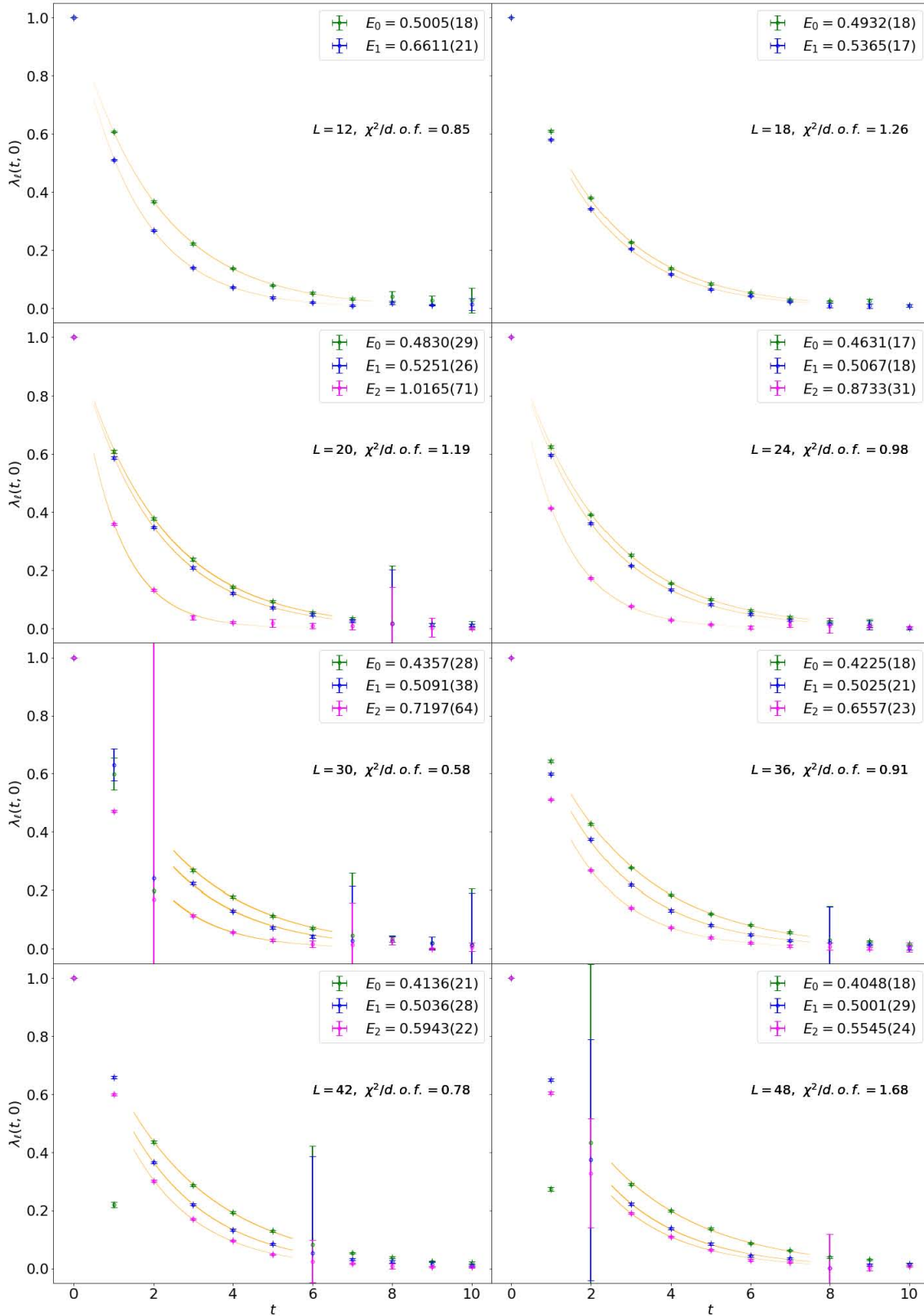


Figure 5.4: Solutions of the GEVP with an exponential fit. Here we consider $g = 0.02$, $\kappa_\varphi = 0.3897$, and $\kappa_\rho = 0.3323$ in order to reproduce the results in [Gattringer and Lang, 1993].

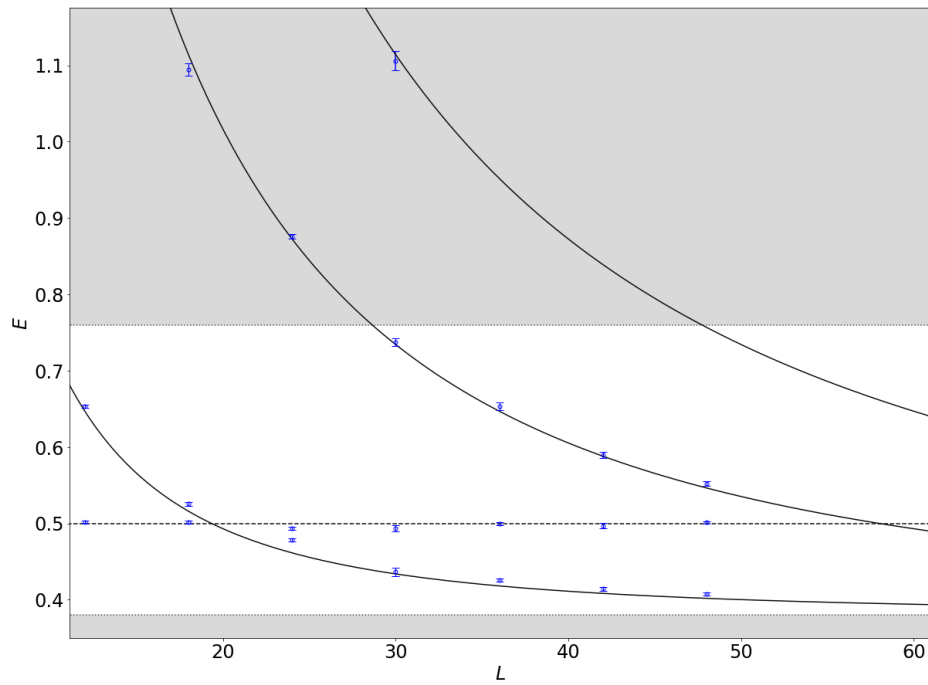


Figure 5.5: Two-particle spectrum for non-resonant scattering. Case I in Table 5.1.

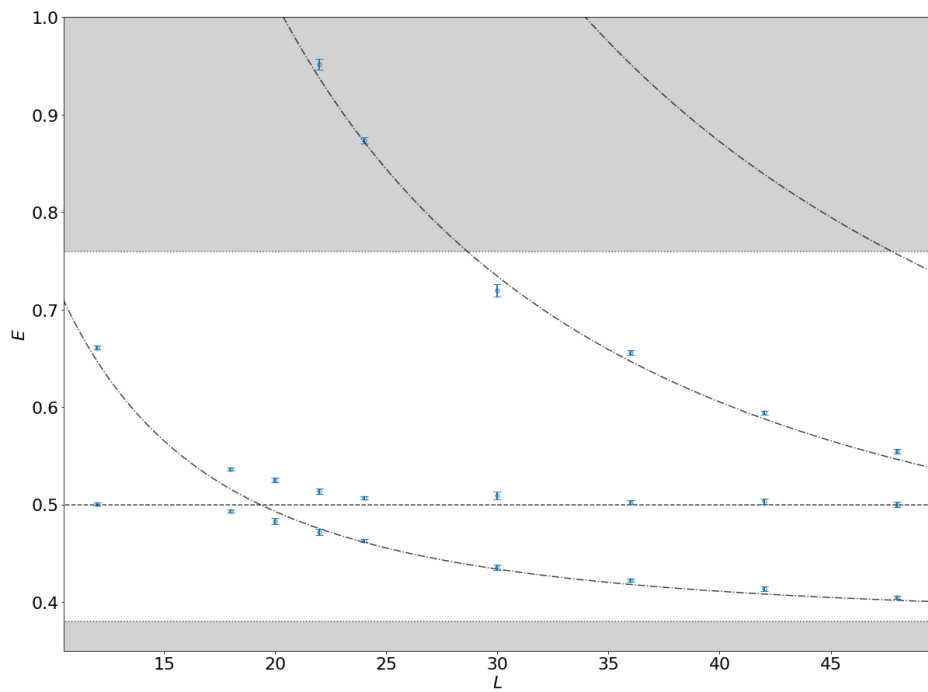


Figure 5.6: Two-particle spectrum for resonant scattering. Case II in Table 5.1.

Part III

Scattering amplitudes and form factors

CHAPTER 6

Infinite volume elastic scattering

In the second part of this thesis we have presented the GL model, as well as reproduced the spectrum of the one- and two-particle sector reported in [Gattringer and Lang, 1993]. In the final part we discuss the outstanding steps towards extracting scattering amplitudes of two-particle states coupling to an external current as proposed by [Briceño and Hansen, 2016], which we review and adapt for 1+1 dimensions in Section 7.1. As a preliminary step we must first extract scattering amplitudes for two-particle states without current insertions. Therefore, we focus on this point in the following sections.

As a step in this direction, in this chapter we go back to the 1+1D Minkowski-type space to review the one- and two-particle propagators of a $\lambda\phi^4$ theory, as well as the relation between the scattering amplitude for two-particle states and the phase-shift. In Section 6.5 we review the scattering problem in finite 2-dimensional spacetime and revisit the finite volume effects with its infinite volume counterpart. Finally, in Chapter 7 we explore a method to extract matrix elements for transition currents between one-particle states.

6.1 Irreducible diagrams

For a $\lambda\phi^4$ field theory the one particle propagator is given as a series of all possible Feynman diagrams with two external legs. Such a series can be written down in terms of the one-particle irreducible (1PI) diagram

$$\text{---} \circlearrowleft \text{---} = \text{---} \text{---} + \text{---} \text{---} + \text{---} \text{---} + \dots, \quad (6.1.1)$$

The fully dressed one-particle propagator can be expressed as the sum to all orders of amputated 1PI diagrams with two external legs

$$\text{---} \bullet \text{---} = \text{---} \text{---} + \text{---} \circlearrowleft \text{---} + \text{---} \circlearrowleft \circlearrowleft \text{---} + \dots, \quad (6.1.2)$$

Similarly, when considering two-particle scattering amplitudes, it is convenient to introduce the sum to all orders of s -channel two-particle irreducible (2PI) diagrams, also known as the

Bethe-Salpeter kernel,

$$\text{Diagram} = \text{Diagram}_1 + \text{Diagram}_2 + \text{Diagram}_3 + \dots \quad (6.1.3)$$

By construction, this is a smooth function in the elastic two-particle region. There can be singularities above the three or four particle thresholds.

6.2 The one-loop term

Here and in Section 6.5, we follow the key steps presented in [Kim et al., 2005] modified to 1+1D. The two-particle scattering amplitude can be expressed as an infinite sum of all $2 \rightarrow 2$ amputated diagrams, and in terms of the Bethe-Salpeter kernel it can be written as

$$i\mathcal{M} = \text{Diagram}_1 + \text{Diagram}_2 + \text{Diagram}_3 + \dots \quad (6.2.1)$$

The loops are formed by connecting two kernels through the fully dressed propagator, which now is drawn simply as a solid line.

The first non-trivial contribution to the scattering amplitude is the one-loop diagram which represents an integral that we denote as I . In order to evaluate the imaginary part of this integral, let us define

$$f(P - k, k) = (iB(P - k, k))^2, \quad (6.2.2)$$

where B is the Bethe-Salpeter kernel. In the kinematic region under consideration ($2m_\varphi < E < 4m_\varphi$) (6.2.2) is a smooth function of its variables. Thus, we can write down the loop integral as

$$I \equiv \text{Diagram} = \int \frac{dk_1}{2\pi} \int \frac{dk_0}{2\pi} \frac{i^2 f(P - k, k)}{[k^2 - m^2 + i\varepsilon][(P - k)^2 - m^2 + i\varepsilon]}. \quad (6.2.3)$$

The k_0 integral can be solved by taking it to the complex plane, see Figure 6.1.

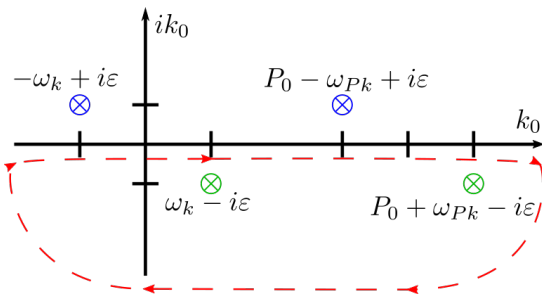


Figure 6.1: The k_0 complex plane. In our case we have decided to close a contour from below.

The poles of the propagators can be expressed in terms of the quantities

$$\begin{aligned} \omega_k &= \sqrt{k_1^2 + m^2}, & \text{and} \\ \omega_{Pk} &= \sqrt{(P_1 - k_1)^2 + m^2}. \end{aligned} \quad (6.2.4)$$

Therefore, solving the k_0 integral is a straightforward application of the Residue Theorem. Now the integral over k_1 has two contributions

$$I = i \int \frac{dk_1}{2\pi} \left\{ \frac{f(\omega_k, k_1)}{2\omega_k [(P_0 - \omega_k)^2 - \omega_{P_k}^2 + i\varepsilon]} + \frac{f(P_0 + \omega_k, k_1)}{2\omega_{P_k} [(P_0 + \omega_{P_k})^2 - \omega_k^2 + i\varepsilon]} \right\}. \quad (6.2.5)$$

At this point it is easier to continue our analysis in the center-of-mass frame, where the coordinates

$$\begin{aligned} k^* &= (\omega_k^*, k_1^*), & P_0 &\rightarrow E^* = \omega_k^* + \omega_{P_k}^*, \\ (P - k)^* &= (\omega_{P_k}^*, -k_1^*), & \omega_k^{*2} &= k_1^{*2} + m^2 = \omega_{P_k}^{*2}, \end{aligned} \quad (6.2.6)$$

are related to the lab-frame through the transformations

$$k_1^* = \gamma(k_1 - \beta\omega_k) \quad \text{and} \quad \omega_k^* = \gamma(\omega_k - \beta k_1), \quad (6.2.7)$$

with $\gamma = E^*/P_0$ and $\beta = P_1/P_0$. The loop integral (6.2.5) takes the form

$$\begin{aligned} I &= I_1 + I_2 = \int \frac{dk_1^*}{2\pi} \frac{\omega_k}{\omega_k^*} \left\{ \frac{f^*(k^*)}{2\omega_k E^* (E^* - 2\omega_k^* + i\varepsilon)} + \frac{f^*(k^*)}{2\omega_{P_k} E^* (E^* + 2\omega_{P_k}^*)} \right\} \\ &= i \int \frac{dk_1^*}{2\pi} \frac{\omega_k}{\omega_k^*} \left\{ \frac{E^* + 2\omega_k^*}{4\omega_k 2E^*} \frac{f^*(k^*)}{q^{*2} - k_1^{*2} + i\varepsilon} + \frac{f^*(k^*)}{2\omega_{P_k} E^* (E^* + 2\omega_{P_k}^*)} \right\}, \end{aligned} \quad (6.2.8)$$

where $q^{*2} = E^{*2}/4 - m^2$. In the last step we have omitted an $i\varepsilon$ term in the second integral because in the elastic scattering region $2m \lesssim E^* \lesssim 3m$, the denominator does not vanish. Therefore, we can focus our attention on the first integral

$$I_1 = i \int \frac{dk_1^*}{2\pi} \frac{E^* + 2\omega_k^*}{4\omega_k^* 2E^*} \frac{f^*(k^*)}{q^{*2} - k_1^{*2} + i\varepsilon}. \quad (6.2.9)$$

Finally we can use the fact that the $i\varepsilon$ regulated propagator can be written as a sum over a Dirac δ -function plus the principal-value piece, whose contribution we denote as $I_{1,\text{PV}}$

$$\begin{aligned} I_1 &= i(-i\pi) \int \frac{dk_1^*}{2\pi} \frac{E^* + 2\omega_k^*}{4\omega_k^* 2E^*} \frac{f^*(k^*) \delta(q^* - k_1^*)}{q^{*2} + k_1^{*2}} + I_{1,\text{PV}} \\ &= [iL^*(q^*)]^* \frac{1}{8E^* q^*} [iR^*(q^*)] + I_{1,\text{PV}}. \end{aligned} \quad (6.2.10)$$

We have split the function carrying the energy-momentum dependence into the contributions from the left and right ends of the loop

$$f^*(q^*) = [iL^*(q^*)]^* [iR^*(q^*)], \quad (6.2.11)$$

and we can identify the (one-dimensional) phase-space as

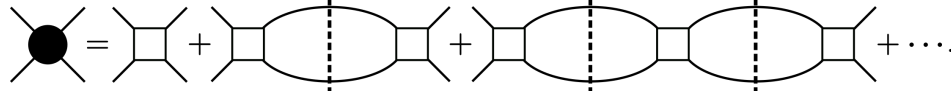
$$\rho_{\text{phase-space}}(q^*) \equiv \frac{1}{8E^* q^*}. \quad (6.2.12)$$

Although not written explicitly, back in (6.2.8) we had switched to the principal value prescription of the second integral, therefore our result for the one-loop diagram can be written as

$$I = I_{\text{PV}} + [iL^*(q^*)]^* \rho_{\text{phase-space}}(q^*) [iR^*(q^*)], \quad (6.2.13)$$

where the I_{PV} term includes the principal value arising from both poles.

the scattering amplitude can be represented more concisely as



$$\text{Diagram} = \text{Diagram}_1 + \text{Diagram}_2 + \text{Diagram}_3 + \text{Diagram}_4 + \dots \quad (6.3.6)$$

Finally, turning to the matrix representation of (6.3.6), it can be represented as

$$i\mathcal{M} = i\mathcal{K} + i\mathcal{K}\rho i\mathcal{K} + i\mathcal{K}\rho i\mathcal{K}\rho i\mathcal{K} + \dots = i\frac{1}{\mathcal{K}^{-1} - i\rho}, \quad (6.3.7)$$

where we have ultimately used the geometric series to simplify the form of the scattering amplitude.

6.4 Implications of the unitarity of the \mathcal{S} -matrix

Unitarity and angular-momentum conservation require the \mathcal{S} -matrix to be a diagonal matrix in angular momentum space and can be expressed in terms of a single real phase as,

$$\mathcal{S}^{(\ell)} = e^{i2\delta_\ell}, \quad (6.4.1)$$

where δ_ℓ is the energy dependent phase shift. At the same time, from its relation with the scattering amplitude, for some initial and final states we have

$$\mathcal{S}^{(\ell)}(n \rightarrow m) = 1 + i2\bar{\rho}\mathcal{M}^{(\ell)}(n \rightarrow m), \quad (6.4.2)$$

where $\bar{\rho}$ is a proportionality constant. Using eqs. (6.4.1) and (6.4.2) we find

$$\mathcal{M}^{(\ell)} = \frac{1}{\bar{\rho}} \frac{e^{i2\delta_\ell} - 1}{2i} = \frac{1}{\bar{\rho} \cot \delta_\ell - i\bar{\rho}}. \quad (6.4.3)$$

Comparing the last equality to our result from summation of all-orders Feynman diagrams of the scattering matrix (6.3.7), we are able to identify

$$\bar{\rho} = \rho \quad \text{and} \quad \mathcal{K}^{-1} = \rho \cot \delta_\ell. \quad (6.4.4)$$

In (6.4.3) we have found a relation between the scattering amplitude and the scattering phase-shift. In a free theory we would expect $\delta_\ell = 0$ while, as a consequence of an interaction, the phase-shift becomes non-trivial.

6.5 Lüscher formalism in 1+1D

Here we rederive the Lüscher formula, which relates the finite-volume spectrum of two particles to their infinite-volume scattering phase shift. As in the previous section, we follow the steps of Ref. [Kim et al., 2005] with the slight modification that this is being done in 1+1 dimensions. The key difference from the analysis of the previous section is that when placed in a finite volume, momentum is discrete. As a result, loops lead to sums rather than integrals. It is our task to identify the dominant difference between finite- and infinite-volume loops. To do this, we will make use of the Poisson summation formula.

The Poisson summation formula relates discrete summations of a function $f(k)$, with $k = (k_0, k_1)$, to its Fourier transform,

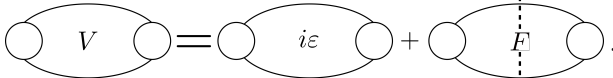
$$\frac{1}{L} \sum_{k_1} f(k) = \sum_l \int \frac{dk_1}{2\pi} e^{iLlk_1} f(k), \quad l \in \mathbb{Z}. \quad (6.5.1)$$

If $f(k)$ is non-singular along the real axis, then the terms $l \neq 0$ decay exponentially as $|k_1| \rightarrow \infty$ and may be neglected. Thus the Poisson summation is reduced to [Lüscher, 1986]

$$\frac{1}{L} \sum_{k_1} f(k) = \int \frac{dk_1}{2\pi} f(k) + \mathcal{O}(e^{-L/r}), \quad (6.5.2)$$

where r is a scale depending on the exact form of $f(k)$ satisfying $L/r \gg 0$. For kinematics where only one-particle states may go on-shell (i.e. $E < 2m_\varphi$) the argument of all the loops present in the correlation functions are non-singular on the real axis. Consequently, from the Poisson summation formula, one can conclude that the corresponding finite-volume corrections are exponentially suppressed [Kim et al., 2005].

If one considers energy above the two-particle threshold (i.e. $E \geq 2m_\varphi$), which is the case in our study, then we have singularities associated with intermediate particles going on-shell. In a finite-volume, these singularities lead to power-law finite-volume effects, and are associated with s -channel two-particle loops [Kim et al., 2005],



$$V = i\varepsilon + F. \quad (6.5.3)$$

Here, V is the finite-volume analogue of the loop defined in (6.2.3) where there are no end-caps present, and F labels the difference between these two and encodes all the power-law finite-volume effects. Given that the singular piece is only the first term in (6.2.5), it is straightforward to see that this is defined as

$$F = \frac{1}{2} \left[\frac{1}{L} \sum_{k_1} - \int \frac{dk_1}{2\pi} \right] \frac{1}{2\omega_k (P - k)^2 - m^2 + i\epsilon}. \quad (6.5.4)$$

It is convenient to use the Poisson summation formula to rewrite (6.5.4) as

$$F = -i\rho \sum_{n \neq 0} e^{iq|n|L} + \mathcal{O}(e^{-mL}). \quad (6.5.5)$$

The $\mathcal{O}(e^{-mL})$ corrections can be safely ignored if $mL \gg 1$, which is a necessary requirement for single-particle states. Following the steps laid out in detail in [Kim et al., 2005], the insertion of (6.5.3) in the finite-volume correlator in momentum space has a singular structure of the form

$$\begin{aligned} C_{2,L} &\sim \frac{1}{\mathcal{K}^{-1} - i\rho \sum_{n \neq 0} e^{iq|n|L}} \\ &= \frac{1}{\rho} \left(\frac{1}{\cot \delta + \cot(qL/2)} \right). \end{aligned} \quad (6.5.6)$$

We have used the results from the infinite-volume analysis of the scattering amplitude (6.4.4) and the fact that

$$\sum_{n \neq 0} e^{iq|n|L} = i \cot(qL/2) - 1. \quad (6.5.7)$$

Finally we find that the poles of the finite-volume correlation function and, consequently, the finite-volume spectra satisfy

$$qL/2 = -\delta + \pi n, \quad (6.5.8)$$

which is the standard result for 1+1D quantum-mechanical systems.

Figure 6.2 displays the phase-shift of the GL model obtained from the two-particle spectrum shown in Figure 5.6 (with $g = 0.02$) through the quantization condition (6.5.8). Although the analysis of phase-shift is still preliminary, the data obtained are consistent with those obtained by [Gattringer and Lang, 1993, Guo, 2013]. At this point, the quantization condition (6.5.8) shows that, by knowing the finite-volume spectrum of the two-particle sector, we can inquire on the phase-shift of the process and thus on the infinite-volume scattering amplitude.

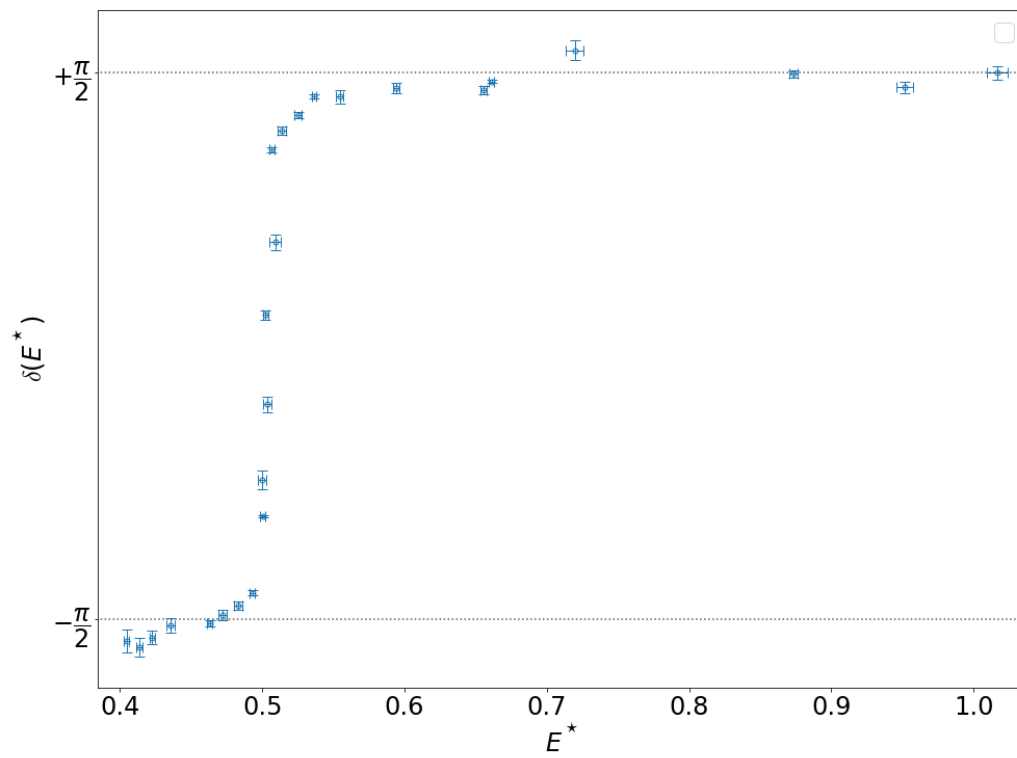


Figure 6.2: Phase-shift of the two-particle scattering in the GL model as obtained from the quantization condition (6.5.8). The length L of the lattice goes from 12 to 48, and we use the parameters from Case II in 5.1.

CHAPTER 7

Finite-volume matrix elements of scalar currents

In this chapter we turn our attention to the main goal of this work, which is to determine the scattering amplitude of two particles coupled to an external current. These amplitudes were first introduced in [Briceño and Hansen, 2016] and were labeled as \mathcal{W}_{df} , where the subscript stands for “*divergence free*”. This emphasizes the fact that these amplitudes are defined as the sum over all diagrams that couple two-particle states with a single current insertion where the poles associated with a single-particle going on-shell have been removed. As discussed in Chapter 1, these amplitudes would allow for the determination of structural information of such states. Here we briefly review the necessary formalism for determining those amplitudes. This formalism, which is schematically depicted by Figure 1.1, was developed in [Briceño and Hansen, 2016, Baroni et al., 2019] for 3+1 dimensional systems.

7.1 Briceño-Hansen formalism in 1+1D

Just as it was the case for the Lüscher formalism discussed in the Section 6.5, it is straightforward to rewrite the formalism of Refs. [Briceño and Hansen, 2016, Baroni et al., 2019] in 1+1D by replacing $L^3 \rightarrow L^1$ and substituting all 3D spatial vectors by 1D spatial vectors. All steps in the derivation are independent of the dimensions. To simplify the discussion further, we assume that the initial and final states are identical and composed of two-particles. Given these simplifications, one finds that the finite-volume matrix elements of a scalar current \mathcal{J} is related to \mathcal{W}_{df} via

$$\left| \langle P, L | \mathcal{J}(0) | P, L \rangle \right| = \frac{\mathcal{R}(P)}{L} \left| \mathcal{W}_{\text{df}}(P^2) + \mathcal{F}(0) (\mathcal{M}(P^2))^2 G(P, L) \right|, \quad (7.1.1)$$

where \mathcal{R} is the Lellouch-Lüscher factor [Lellouch and Lüscher, 2001, Briceño et al., 2015], which is related to the derivative of \mathcal{M} and F ,

$$\mathcal{R}(P) \equiv \lim_{E \rightarrow E_n} \left[\frac{E - E_n}{F^{-1}(P, L) + \mathcal{M}(P^2)} \right], \quad (7.1.2)$$

G is a new finite-volume function that is closely related to the F function,

$$G(P, L) \equiv \left[\frac{1}{L} \sum_n - \int \frac{dk_1}{2\pi} \right] \frac{1}{2\omega_k} \left(\frac{1}{(P - k)^2 - m^2 + i\varepsilon} \right)^2, \quad (7.1.3)$$

and finally \mathcal{F} is the one-particle form factor. This is in general a function of the virtuality, Q^2 , of the current. Because in (7.1.1) we have focused our attention on the case where the current carries no virtuality, the argument of the form factor is zero.

In summary, (7.1.1) tells us that given the pieces itemized in the introduction, Chapter 1, one can obtain the desired \mathcal{W}_{df} function. In the previous chapter we have demonstrated that the spectrum is accessible from the two-point Euclidean correlators. We performed calculations of these correlators for the GL model in Chapter 5. In the remainder of this chapter we review how the single particle form factors can be extracted from three-point correlation functions. We carry out an exploratory study of possible choices for scalar currents to consider, and we present preliminary results for the single particle form factors for these choices. Just as is the case for the spectrum, the finite-volume errors for the single particle matrix elements scale as $\mathcal{O}(e^{-mL})$ and will be neglected in what follows.

7.2 Three-point correlators of one-particle states

In Section 3.2 we reviewed how the two-point correlation functions can be expressed as the spectral decomposition of the vacuum. A similar analysis allows us to study the three-point correlators for a transition current \mathcal{J} ,

$$\begin{aligned} C_{fi}^{3pt}(t_f, t_c, t_i) &= \langle \Omega | \tilde{\mathcal{O}}(f, t_f) \tilde{\mathcal{J}}(q, t_c) \tilde{\mathcal{O}}^\dagger(i, t_i) | \Omega \rangle \\ &= \sum_{n_f, n_i} \frac{e^{-E_{n_f}(p_f)(t_f - t_c)} \mathcal{Z}_f^{(n_f)*}}{2LE_{n_f}(p_f)} \frac{e^{-E_{n_i}(p_i)(t_c - t_i)} \mathcal{Z}_i^{(n_i)}}{2LE_{n_i}(p_i)} \langle n_f; p_f | \tilde{\mathcal{J}}(q, 0) | n_i; p_i \rangle, \end{aligned} \quad (7.2.1)$$

where $n_i, n_f \in \mathbb{Z}$ and $\tilde{\mathcal{J}}$ is the Fourier transform of \mathcal{J} , defined as

$$\tilde{\mathcal{J}}(q, t) = \sum_{x_1} \mathcal{J}(x_1, t) e^{ix_1 q}. \quad (7.2.2)$$

Here we can identify the overlaps and the energy levels from the one-particle sector as seen in Section 5.2. Therefore, the acquired knowledge from the one-particle states, i.e. the parameters \mathcal{A} in (5.2.4) obtained from fitting the one-particle correlators, allows us to study the transition matrix elements of a given current

$$C_{fi}^{3pt}(t_f, t_c, 0) = \frac{e^{-E_{0_f}(p_f)(t_f - t_c)} \sqrt{\mathcal{A}_f}}{\sqrt{2LE_{0_f}(p_f)}} \frac{e^{-E_{0_i}(p_i)(t_c)} \sqrt{\mathcal{A}_i}}{\sqrt{2LE_{0_i}(p_i)}} \langle 1; p_f | \tilde{\mathcal{J}}(q, 0) | 1; p_i \rangle, \quad (7.2.3)$$

where we are considering the contributions from excited states to be negligible, and set $t_i = 0$.

Now, through its inverse Fourier transform, the matrix element of $\tilde{\mathcal{J}}(q, 0)$ can be expressed as

$$\langle 1; p_f | \tilde{\mathcal{J}}(q, 0) | 1; p_i \rangle = L \mathcal{F}(Q^2) \delta_{n_q, n_f - n_i}, \quad \text{with} \quad \mathcal{F}(Q^2) \equiv \langle 1; p_f | \mathcal{J}(0, 0) | 1; p_i \rangle, \quad (7.2.4)$$

where $\mathcal{F}(Q^2)$ is defined as a form factor and $Q^2 = p_i^2 - p_f^2$. Substituting this result in (7.2.3) and solving for the form factor, we obtain

$$\mathcal{F}(Q^2) = \sqrt{\frac{2E_{0_f}(p_f)}{\mathcal{A}_f}} \sqrt{\frac{2E_{0_i}(p_i)}{\mathcal{A}_i}} e^{E_{0_f}(p_f)(t_f-t_c)} e^{E_{0_i}(p_i)(t_c)} C_{f_i}^{3pt}(t_f, t_c, 0). \quad (7.2.5)$$

It should be noticed that, while the three-point correlator $C_{f_i}^{3pt}$ is a new quantity to be evaluated on the lattice, everything else on the right-hand side of (7.2.5) can be extracted from an analysis of the one-particle sector along the lines of Section 5.2. Also, since \mathcal{F} does not depend on time, the exponential factors on the right-hand side must cancel with the time dependence of the three-point correlators.

7.3 Smearred operators

In order to explore transitions between one-particle states in the GL model, it is necessary to extract matrix elements for the possible currents. The simplest options of currents for one-to-one transitions are

$$\varphi + \rho \rightarrow \varphi' \quad \text{and} \quad \varphi + \varphi^2 \rightarrow \varphi''. \quad (7.3.1)$$

However, the latter would seem to be a rather trivial current since $\varphi^2 = 1$ in the GL model. Also ρ only takes the values ± 1 values. Such limitation may be circumvented by means of smeared operators. In fact, in the action of the GL model (3.1.1), one of the φ fields was smeared as the average of the nearest neighbors of the φ field on the lattice site x

$$g\rho(x)\varphi(x)\bar{\varphi}(x) = \frac{g}{2}\rho(x)\varphi(x) \sum_{\mu} [\varphi(x + \hat{\mu}) - \varphi(x - \hat{\mu})], \quad (7.3.2)$$

otherwise the action would not be sensible to the interactions between the two types of fields.

A Gaussian smearing with truncated boundary conditions

$$\bar{\varphi}_{\sigma}(x_1, t) = \sum_{y_1} \varphi(y_1, t) e^{-(x_1 - y_1)^2 / 2\sigma^2}, \quad (7.3.3)$$

offers a more sophisticated approach for our study of transition matrix elements since it allows us to consider couplings with fields in a broader region around the lattice site x . The parameter σ is fixed and it controls the number of sites for which the coupling is more intense. In Figure 7.1 we illustrate how a smeared operator is evaluated on a sample configuration.

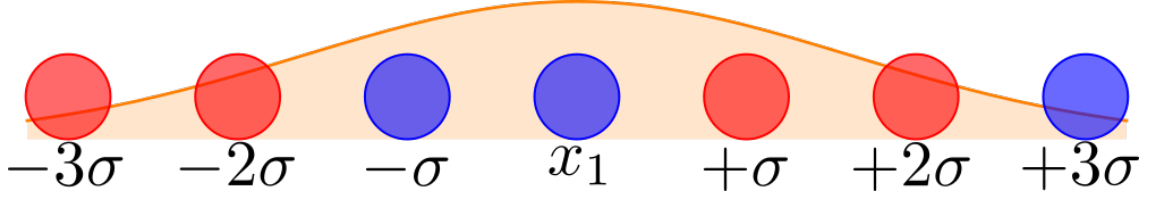


Figure 7.1: Gaussian distribution centered at x_1 , with unit σ . Thus, the n -th order neighbors are located at a distance n from x_1 .

7.4 Matrix elements

In terms of the smeared operator, the φ^2 transition current has the form

$$\mathcal{J}_\sigma(x) = \varphi(x)\bar{\varphi}_\sigma(x), \quad (7.4.1)$$

and the corresponding Fourier transform reads

$$\tilde{\mathcal{J}}_\sigma(n, t) = \sum_{x_1} \mathcal{J}_\sigma(x_1, t) e^{ix_1 p_n}. \quad (7.4.2)$$

The three-point correlators for one-to-one matrix elements are evaluated on the lattice analogously to the two-point correlators. The difference is that now we have an operator representing the transition current which is evaluated at an interaction time such that $0 < t_c < t_f$. For a given configuration the three-point Euclidean correlator reads

$$C_{fi}^{3pt}(t_f, t_c, 0) = \tilde{\varphi}(f, t_f) \tilde{\mathcal{J}}_\sigma(n_q, t_c) \tilde{\varphi}(i, 0). \quad (7.4.3)$$

Thus the first and third factors correspond to one-particle momentum operators at the t_f -th and 0-th correlation time, respectively, while the second factor, thus the current, is given by (7.4.2) with $n_q = f - i$.

The three-point correlator for this one-to-one current can be evaluated on the lattice using the same operators as in the one- and two-particle sector for the initial and final states, and the smeared current (7.4.1), respectively. Then, from (7.2.5), we can extract the matrix element of the transition current for given initial and final states with momenta p_i and p_f , respectively. Ultimately, the form factor for this current can be constructed as a function of the virtuality

$$Q^2 = -q^2 = \frac{4\pi^2}{L^2} (n_f - n_i)^2 - (E_f - E_i)^2 \quad (7.4.4)$$

Again, from evaluating all of the available configurations it is possible to obtain a JK-ensemble of three-point correlators

$$\{C_{fi}^{3pt}(t_f, t_c, 0)\}_N^{JK}$$

which is related to the transition current matrix elements through (7.2.5) and (7.2.4), thus

$$\{C_{fi}^{3pt}\}_N^{JK} \rightarrow \{\mathcal{F}(Q^2)\}_N^{JK}.$$

In Figure 7.2, we show plots of preliminary results for the form factors of the currents considered here. In each panel, we show the form factor obtained for different combinations of the initial and final state momentum. The form factors are normalized by fixing the mean value of the matrix elements of the lowest-lying state to be 1. These are plotted as functions of the current insertion time and for two choices of the final state time, convincingly showing that excited state contaminations are statistically negligible.

In the different graphs, we consider different possibilities of the smearing width. As one would expect, by taking the smearing to zero, we recover the diagonal behavior of the form factors in momentum space. It is evident that by choosing a larger smearing width, one obtains non-zero values of the form factors for non-zero virtuality of the current. We cannot ascertain if this behavior will affect the two-particle matrix elements. Therefore, if the effect of the off-diagonal matrix elements in the one-particle sector is relevant for the two-particle sector, right now the only way we can account for this possibility is through our smeared current. Then we would have to explore the limit when the smearing goes to zero in the two-particle sector. As a result, we conclude that this is a promising direction for performing exploratory calculations of currents in this scalar field theory.

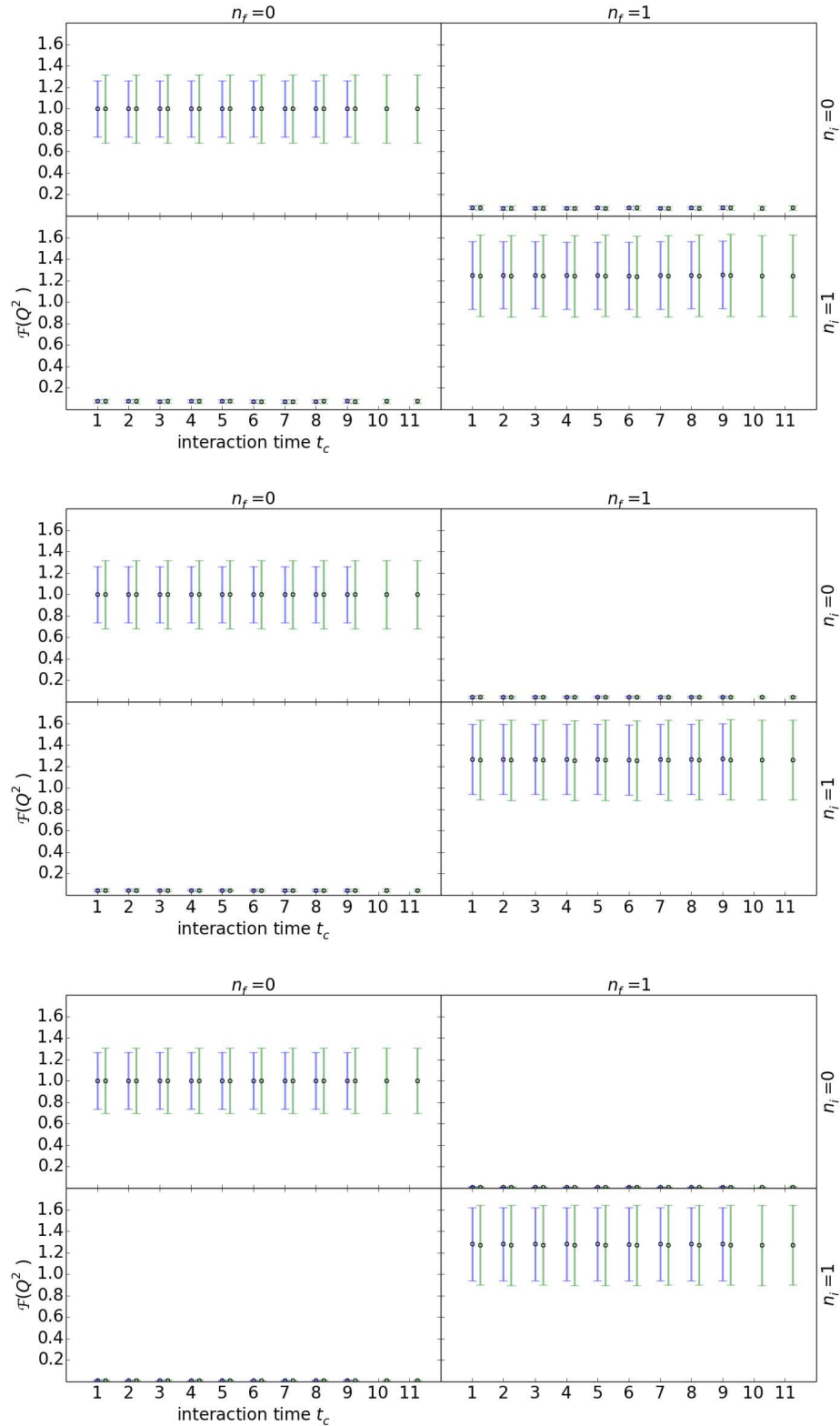


Figure 7.2: Matrix elements for smeared φ^2 currents in the GL model for separation times $\Delta t = 10$ (in blue) and $\Delta t = 12$ (in green). Top to bottom $\sigma = 1.5, 1, 0.5$, $L = 42$ with the parameters used in the coupled scenario, Case II in Table 5.1.

CHAPTER 8

Conclusion

The purpose of this thesis has been to explore the applicability of the Briceño-Hansen formalism in a lattice field theory, see Chapter 1. The formalism presented in [Briceño and Hansen, 2016, Baroni et al., 2019] describes the relation between finite-volume two-particle matrix elements and the transition amplitudes between two-particle states coupled to an external current. In Section 7.1 we have presented the Briceño-Hansen formalism in $1 + 1D$, see (7.1.1). The application of this formalism to the model considered here requires four pieces to be determined from the lattice: 1) the spectrum of one-particle states, 2) the spectrum of two-particle states, 3) the matrix elements of one-particle states, and 4) the matrix elements of two-particle states, cf. 1.

For the first two points we have reproduced some of the results reported by [Gattringer and Lang, 1993]. In Chapter 5, we have extracted the spectrum for one- and two-particle states from the analysis of correlation functions. In Section 6.5 we obtained the scattering phase-shift following the Lüscher formalism [Lüscher and Wolff, 1990]. At this point we could be confident that the simulation algorithm and the analysis of correlation functions were implemented correctly.

As for the third point, in Section 7.4 we were able to obtain matrix elements for one-particle states. To achieve this, we defined a current \mathcal{J}_σ that can account for the transition between one-particle states with different momenta. This required the use of the smeared operators defined in (7.4.1). As $\sigma \rightarrow 0$ the diagonal behavior of the currents is recovered. The immediate step is to determine the form factors for a range of virtualities using different boosts and volumes. Then we would be able to proceed to study two-particle matrix elements. For this, we would need to evaluate the corresponding three-point correlation functions using the interpolators for two-particle states obtained in Section 5.3.

Finally, upon calculation of the Lellouch-Lüscher factor (7.1.2) and the G function (7.1.3), we will have all the necessary pieces to implement the Briceño-Hansen formalism in a lattice field theory for the first time. In this way, we will be able to access the infinite-volume transition amplitude for two-particle φ states, which automatically allows us to know about the structure of the resonant state labeled here as ρ . This will be useful for future QCD studies since it will provide an empirical confirmation of a formalism with the capability of extracting structural information of multi-particle hadronic states via lattice QCD.

Appendix

APPENDIX A

Jackknife statistics

The jackknife resampling method avoids the difficulties arising from Gaussian error propagation while providing a more convenient and realistic method for error estimation.

a_1	a_2	a_3	$X^{(1)}$	a_1	a_2	a_3	$X^{(1)}$	a_1	a_2	a_3	$X^{(1)}$
a_4	a_5	a_6	$X^{(2)}$	a_4	a_5	a_6	$X^{(2)}$	a_4	a_5	a_6	$X^{(2)}$
a_7	a_8	a_9	$X^{(3)}$	a_7	a_8	a_9	$X^{(3)}$	a_7	a_8	a_9	$X^{(3)}$
a_{10}	a_{11}	a_{12}	$X^{(4)}$	a_{10}	a_{11}	a_{12}	$X^{(4)}$	a_{10}	a_{11}	a_{12}	$X^{(4)}$
a_{13}	a_{14}	a_{15}	$X^{(5)}$	a_{13}	a_{14}	a_{15}	$X^{(5)}$	a_{13}	a_{14}	a_{15}	$X^{(5)}$

Table A.1: A list of 15 values divided into 5 bins. From left to right, the highlighted values are averaged to compute the first, second and third elements of the JK-ensemble.

A.1 Bins, jackknife ensembles and errors

Let A represent an ordered list of m values

$$A = \{a_1, a_2, \dots, a_m\}. \quad (\text{A.1.1})$$

This list can be divided into n bins, denoting the i -th bin as $X^{(i)}$, with m/n values each, provided that the total number of values can be exactly divided by n . Then the initial list (A.1.1) can be resampled into a jackknife ensemble (JK-ensemble) whose elements are given by the average of all values, excluding those values contained within a bin of the original ensemble,

$$A^{JK} = \{A_1^{JK}, A_2^{JK}, \dots, A_n^{JK}\}, \quad \text{with} \quad A_i^{JK} = \frac{n}{m(n-1)} \sum_{j \notin X^{(i)}} a_j. \quad (\text{A.1.2})$$

Table A.1 illustrates this procedure with a list of 15 values divided into 5 bins.

Let \bar{A} be the mean value of the entire set. The variance of the JK-ensemble is computed as

$$\sigma_A^2 \equiv \frac{n-1}{n} \sum_{i=1}^n (A_i^{JK} - \bar{A})^2. \quad (\text{A.1.3})$$

The square root of this quantity gives an estimate for the error of the mean value of list (A.1.1). One can finally quote the expected value for the observable to be determined from list (A.1.1) as

$$\langle A \rangle = \bar{A} \pm \sigma_A. \quad (\text{A.1.4})$$

A.2 Observables and covariance

In practice, the observables to be determined are not only averages but functions of their mean values. In such cases the jackknife method can still be used to determine the errors of those observables. Consider a parameter given as a function of the expected value of list (A.1.1), $F(\langle A \rangle)$. Knowing the function we can generate a JK-ensemble for the observable F

$$F^{JK} = \{F_1^{JK}, F_2^{JK}, \dots, F_n^{JK}\} \quad \text{with} \quad F_i^{JK} = F(A_i^{JK}). \quad (\text{A.2.1})$$

Then eqs. (A.1.3) to (A.1.4) allow us to know the expected value of F and its uncertainty without resorting to Gaussian error propagation.

Furthermore, in many cases we have to perform fits over quantities like $\langle A \rangle$ or $\langle F \rangle$ which may be correlated to each other. In order to take correlation effects into account, knowledge of the covariance between the variables is necessary. For example, let B and C be variables determined from lists of data; the covariance between these variables can be obtained from their respective JK-ensembles. Thus, provided B^{JK} and C^{JK} , the covariance coefficient between these variables is given by

$$\sigma_B \sigma_C = \frac{n-1}{n} \left[\sum_{i=1}^n (B_i^{JK} - \bar{B}) \right] \left[\sum_{i=1}^n (C_i^{JK} - \bar{C}) \right]. \quad (\text{A.2.2})$$

Ultimately, the covariance coefficients between all of the considered variables form a matrix that can be considered in fitting methods such as the χ^2 -regression.

Bibliography

- [Baroni et al., 2019] Baroni, A., Briceño, R. A., Hansen, M. T., and Ortega-Gama, F. G. (2019). Form factors of two-hadron states from a covariant finite-volume formalism. *Phys. Rev.*, D100(3):034511.
- [Briceño, 2013] Briceño, R. A. (2013). On the Determination of Elastic and Inelastic Nuclear Observables from Lattice QCD. PhD thesis, Washington U., Seattle.
- [Briceño et al., 2018] Briceño, R. A., Dudek, J. J., and Young, R. D. (2018). Scattering processes and resonances from lattice QCD. *Rev. Mod. Phys.*, 90(2):025001.
- [Briceño et al., 2016] Briceño, R. A. et al. (2016). Issues and Opportunities in Exotic Hadrons. *Chin. Phys.*, C40(4):042001.
- [Briceño and Hansen, 2016] Briceño, R. A. and Hansen, M. T. (2016). Relativistic, model-independent, multichannel $2 \rightarrow 2$ transition amplitudes in a finite volume. *Phys. Rev.*, D94(1):013008.
- [Briceño et al., 2019] Briceño, R. A., Hansen, M. T., and Jackura, A. W. (2019). Consistency checks for two-body finite-volume matrix elements: I. Conserved currents and bound states. [arXiv:hep-lat/1909.10357](https://arxiv.org/abs/1909.10357).
- [Briceño et al., 2015] Briceño, R. A., Hansen, M. T., and Walker-Loud, A. (2015). Multichannel $1 \rightarrow 2$ transition amplitudes in a finite volume. *Phys. Rev.*, D91(3):034501.
- [Chen et al., 2016] Chen, H.-X., Chen, W., Liu, X., and Zhu, S.-L. (2016). The hidden-charm pentaquark and tetraquark states. *Phys. Rept.*, 639:1–121.
- [Dudek et al., 2008] Dudek, J. J., Edwards, R. G., Mathur, N., and Richards, D. G. (2008). Charmonium excited state spectrum in lattice QCD. *Phys. Rev. D*, 77:034501.
- [Forcrand et al., 2004] Forcrand, P., García Pérez, M., Matsufuru, H., Nakamura, A., Pushkina, I., Stamatescu, I.-O., Takaishi, T., and Umeda, T. (2004). Contribution of disconnected diagrams to the hyperfine splitting of charmonium. *JHEP*, 2004(08):004–004.
- [Gattringer and Lang, 1993] Gattringer, C. and Lang, C. (1993). Resonance scattering phase shifts in a 2d lattice model. *Nucl. Phys. B*, 391(1):463 – 482.
- [Gattringer and Lang, 2010] Gattringer, C. and Lang, C. B. (2010). Quantum Chromodynamics on the Lattice. *Lect. Notes Phys.*, 788.

- [Guo et al., 2018] Guo, F.-K., Hanhart, C., Meißner, U.-G., Wang, Q., Zhao, Q., and Zou, B.-S. (2018). Hadronic molecules. *Rev. Mod. Phys.*, 90(1):015004.
- [Guo, 2013] Guo, P. (2013). Coupled-channel scattering in 1+1 dimensional lattice model. *Phys. Rev. D*, 88:014507.
- [Guo and Gasparian, 2018] Guo, P. and Gasparian, V. (2018). Numerical approach for finite volume three-body interaction. *Phys. Rev.*, D97(1):014504.
- [Itzykson and Drouffe, 1989] Itzykson, C. and Drouffe, J.-M. (1989). *Statistical Field Theory*, volume 1, Cambridge Monographs on Mathematical Physics. Cambridge University Press.
- [Kim et al., 2005] Kim, C., Sachrajda, C., and Sharpe, S. R. (2005). Finite-volume effects for two-hadron states in moving frames. *Nucl. Phys. B*, 727(1):218 – 243.
- [Lebed et al., 2017] Lebed, R. F., Mitchell, R. E., and Swanson, E. S. (2017). Heavy-Quark QCD Exotica. *Prog. Part. Nucl. Phys.*, 93:143–194.
- [Lellouch and Lüscher, 2001] Lellouch, L. and Lüscher, M. (2001). Weak transition matrix elements from finite volume correlation functions. *Commun. Math. Phys.*, 219:31–44.
- [Liu, 2014] Liu, X. (2014). An overview of *XYZ* new particles. *Chin. Sci. Bull.*, 59:3815–3830.
- [Lüscher, 1986] Lüscher, M. (1986). Volume Dependence of the Energy Spectrum in Massive Quantum Field Theories. 1. Stable Particle States. *Commun. Math. Phys.*, 104:177.
- [Lüscher, 1991] Lüscher, M. (1991). Two particle states on a torus and their relation to the scattering matrix. *Nucl. Phys. B*, B354:531–578.
- [Lüscher and Weisz, 1987] Lüscher, M. and Weisz, P. (1987). Scaling laws and triviality bounds in the lattice ϕ^4 theory: (i). One-component model in the symmetric phase. *Nucl. Phys. B*, 290:25 – 60.
- [Lüscher and Wolff, 1990] Lüscher, M. and Wolff, U. (1990). How to calculate the elastic scattering matrix in two-dimensional quantum field theories by numerical simulation. *Nucl. Phys. B*, 339(1):222 – 252.
- [Rummukainen and Gottlieb, 1995] Rummukainen, K. and Gottlieb, S. (1995). Resonance scattering phase shifts on a non-rest-frame lattice. *Nucl. Phys. B*, 450(1):397 – 436.
- [Schwartz, 2014] Schwartz, M. D. (2014). *Quantum Field Theory and the Standard Model*. Cambridge University Press.
- [Swendsen and Wang, 1987] Swendsen, R. H. and Wang, J.-S. (1987). Nonuniversal critical dynamics in Monte Carlo simulations. *Phys. Rev. Lett.*, 58:86–88.